

# 7-Methoxytacrine and 2-Aminobenzothiazole Heterodimers: Structure–Mechanism Relationship of Amyloid Inhibitors Based on Rational Design

Miroslav Gancar,<sup>+</sup> Kiet Ho,<sup>+</sup> Sk. Abdul Mohid, Nguyen Quoc Thai, Zuzana Bednarikova, H. Linh Nguyen, Anirban Bhunia, Eugenie Nepovimova, Mai Suan Li,\* and Zuzana Gazova\*



Cite This: *ACS Chem. Neurosci.* 2020, 11, 715–729



Read Online

ACCESS |

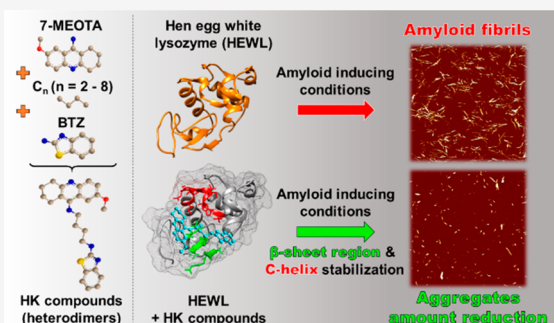
Metrics & More

Article Recommendations

Supporting Information

**ABSTRACT:** The formation and accumulation of amyloid aggregates are the phenomena that accompany amyloidoses, which are currently untreatable and include Alzheimer's and Parkinson's diseases, diabetes mellitus, non-neuropathic lysozyme systemic amyloidosis, and others. One of the very promising therapeutic approaches seems to be an inhibition of amyloid formation and/or clearance of amyloid aggregates. Small molecules have a great potential to interfere with amyloid fibrillation of peptides and polypeptides, which can be improved by connection of cyclic structures into single multicyclic molecules and their dimerization. In our study, we focused on heterodimers consisting of 7-methoxytacrine (7-MEOTA) and 2-aminobenzothiazole (BTZ) parent molecules connected by an aliphatic linker. Using *in vitro* and *in silico* methods, we investigated the ability of studied compounds to inhibit the amyloid aggregation of hen egg white lysozyme. Heterodimerization led to significant improvement of inhibitory activity compared to that of the parent molecules. The efficiency of the heterodimers varied; the most effective inhibitor contained the longest linker, eight carbons long. We suggest that binding of a heterodimer to a lysozyme blocks the interaction between the  $\beta$ -domain and C-helix region essential for the formation of amyloid cross- $\beta$  structure. Elongation of the linker ultimately enhances the compound's ability to prevent this interaction by allowing the BTZ part of the heterodimer to bind more effectively, increasing the compound's binding affinity, and also by greater steric obstruction. This study represents an important contribution to the recent rational design of potential lead small molecules with anti-amyloid properties, and the heterodimers studied are prospective candidates for the treatment of systemic lysozyme amyloidosis and other amyloid-related diseases.

**KEYWORDS:** Protein aggregation, amyloid, heterodimerization, inhibition, lysozyme, small molecules



## INTRODUCTION

After decades of research, protein amyloid aggregation remains one of the biggest challenges for the scientific community because of its association with amyloid-related diseases as well as recently obtained knowledge that protein amyloids also play physiological roles in organisms. Now, it is believed all peptide and polypeptide sequences can adopt the amyloid state under appropriate conditions.<sup>1</sup> Although the precise molecular mechanism of amyloid aggregation *in vivo* is still unknown, there are a lot of factors affecting the propensity of peptides and polypeptides to be transformed from a soluble state into almost insoluble amyloid structures. They include genetic mutations, post-translational modifications, high protein concentration, and the presence of metal ions.<sup>2</sup> *In vitro* exposure of proteins to amyloid-inducing conditions such as high temperature or protein concentration, pH, and the presence of salts or denaturants results in the formation of

amyloid fibrils with cross- $\beta$  architecture common to amyloid aggregates formed *in vivo*.

It is generally accepted that the formation and accumulation of amyloid deposits in various tissues can have a toxic effect on different cell types, leading to cell dysfunction. Amyloidosis can represent a serious health problem leading to life-threatening organ failure and finally, death.<sup>3</sup> Alzheimer's and Parkinson's diseases, the most common forms of dementia, as well as diabetes mellitus are some of the more than 50 currently known amyloid diseases. Human lysozyme is associated with lysozyme hereditary systemic non-neuropathic amyloidosis. It has been reported that amyloidogenic variants of the human

Received: July 29, 2019

Accepted: February 3, 2020

Published: February 3, 2020

lysozyme are encoded by six different mutations of the lysozyme gene. The phenotype of lysozyme systemic amyloidosis is heterogeneous and includes gastrointestinal symptoms, sicca syndrome, hepatic rupture, petechiae and purpura, renal failure, and lymphadenopathy.<sup>4,5</sup> Hen egg white lysozyme (HEWL) represents an interesting model system to investigate formation of amyloid aggregates and identify novel inhibitors with potential to deal with this disease. This 129-residue-long anti-bacterial protein has been extensively used in studies as its structure and folding properties are well known and it is highly homologous to human lysozyme. *In vitro*, it undergoes amyloid aggregation when exposed to high temperatures in acidic conditions.<sup>6,7</sup>

Currently, there is no cure for amyloid diseases. Treatment is mainly focused on alleviating symptoms, thus improving the quality of the patient's life. Therefore, a great emphasis is placed on the development of effective strategies for their successful treatment. One of the prospective therapeutic approaches involves inhibition of amyloid fibrillization or clearance of amyloid aggregates.

Many small molecules have proved to be capable of inhibition of amyloid aggregation. Most of the studied compounds possess structural features known to be important for their interaction with core regions of early-formed amyloid species and mature amyloid fibrils. These characteristics include the presence of aromatic rings, the substitution pattern of these aromatics, and the length and flexibility of the linker connecting the functional groups.<sup>8–10</sup> Curcumin and its derivatives exhibit the ability to interfere with  $\beta$ -amyloid fibrils and aggregates.<sup>8,11</sup> Derreumaux et al. reported the effects of many drugs targeting mainly  $A\beta$  peptide obtained from *in vitro* and *in vivo* experiments and clinical trials.<sup>12,13</sup> Glyco-acridines inhibit amyloid aggregation of human insulin as well as HEWL.<sup>14,15</sup> Siddiqi et al. showed that capreomycin effectively suppresses the insulin amyloid fibrillization.<sup>16</sup> The ability of polyphenols to affect the amyloid aggregation of HEWL *in vitro* has been reported.<sup>17</sup>

Tacrine was the first cholinesterase inhibitor approved by the U.S. FDA and also one of the most popular aromatic structures tested for possible anti-amyloid properties. However, its use has been restricted due to its hepatotoxicity.<sup>18,19</sup> Therefore, the search for more effective, secure, and multi-functional tacrine derivatives is still of interest.<sup>8</sup> It has been demonstrated that the tacrine analogue 7-methoxytacrine (7-MEOTA) and its derivatives have the ability to inhibit the amyloid formation of  $A\beta_{1-40}$  peptide while being less toxic than but having pharmacological activity equal to that of tacrine.<sup>19,20</sup> The other interesting molecule is benzothiazole—one of the most important chemical structures featured in a variety of natural and pharmaceutical agents—and its derivatives.<sup>21</sup>

Heterodimerization remains an attractive concept leading to preservation, combination, or improvement of beneficial biological properties of parent compounds. It is believed that it is a valid concept when dealing with diseases as complex as amyloidoses. Furthermore, it provides an opportunity to take advantage of the active linker region which connects parent molecules and, thus, enhance the effects of uniquely designed anti-amyloid compounds.<sup>9,22</sup>

In this paper, we focus on the effects of hybrid heterodimers on amyloid aggregation of HEWL. A novel series of heterodimers (HK compounds) was prepared through linkage of functional molecules 7-MEOTA and 2-aminobenzothiazole

(BTZ) using aliphatic linkers varying in length. The results obtained using various *in vitro* and *in silico* biophysical methods show that HK compounds are capable of effective dose-dependent inhibition of HEWL amyloid aggregation at acceptable toxicity levels. It was found that heterodimerization greatly improves the anti-amyloid ability of the parent compounds. Moreover, we investigated the structure–activity relationships of the studied molecules. Binding of heterodimers to HEWL mostly depends on a compound's aromatic groups and leads to blocking of the interaction between the  $\beta$ -domain and C-helix regions essential for formation of amyloid cross- $\beta$  structure. Despite this fact, the length of the linker is a decisive factor among the HK compounds in terms of their affinity to HEWL as well as their inhibitory activity.

## RESULTS AND DISCUSSION

Heterodimerization of small molecules represents a novel approach allowing researchers to improve anti-amyloid activities of compounds. We synthesized heterodimeric 7-MEOTA–BTZ molecules (HK compounds 1066, 1068, 1070, and 1072) by linking parent molecules 7-MEOTA and BTZ using variable length aliphatic linkers ( $C_n$ ;  $n = 2, 4, 6$ , or 8). The chemical structures of the compounds are displayed in Table 1. The parent molecules (7-MEOTA and BTZ) as well

**Table 1. 2D and 3D Structures of Studied Parent Molecules 7-MEOTA and BTZ and Synthesized Heterodimeric HK Compounds**

Name	2D structure	3D structure
7-MEOTA		
BTZ		
HK 1066		
HK 1068		
HK 1070		
HK 1072		

as four heterodimers were investigated to determine whether they are able to inhibit HEWL amyloid aggregation. *In vitro* and *in silico* experiments were used to examine their mechanism of action and to identify relationships between the molecular structure of heterodimers and their inhibitory activity.

**Inhibition of HEWL Amyloid Fibrils Formation and Determination of IC<sub>50</sub> Values.** The ability of the studied compounds to inhibit amyloid aggregation of HEWL was examined using the Thioflavin T (ThT) based fluorescence assay. The extent of inhibition of amyloid fibrillization was

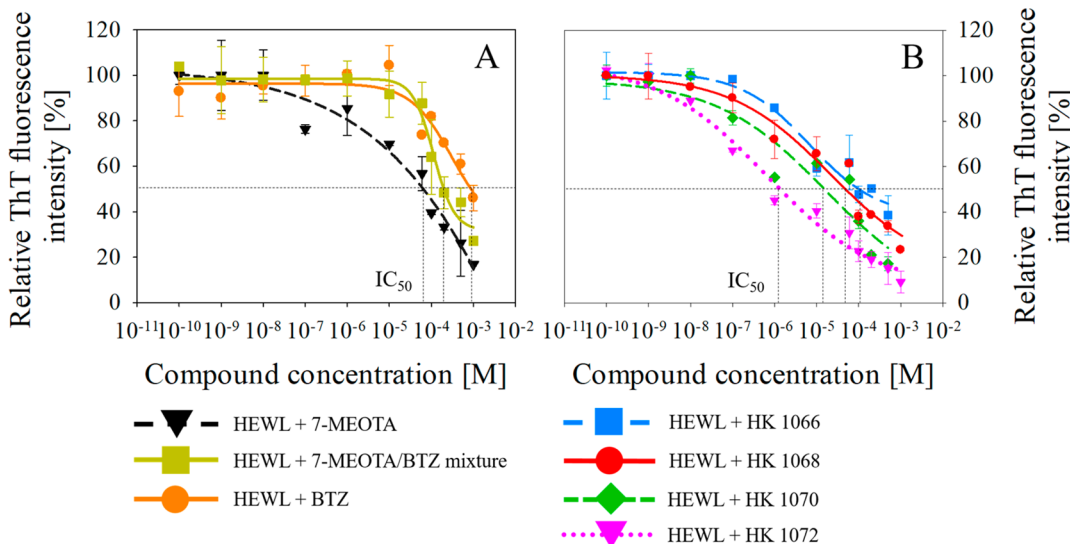


**Figure 1.** ThT fluorescence intensities of HEWL fibrillization in the presence of increasing concentrations of (A) 7-MEOTA (black triangles), BTZ (orange circles), and their equimolar mixture (dark yellow squares), and (B) HK 1066 (blue squares), HK 1068 (red circles), HK 1070 (green diamonds), and HK 1072 (magenta triangles). ThT fluorescence intensities were normalized to fluorescence of 10  $\mu$ M HEWL fibrils formed without added compounds (taken as 100%). Experiments were performed as three independent measurements ( $n = 3$ ); error bars represent the average deviation of three separate samples.

studied for all six compounds individually and an equimolar mixture of 7-MEOTA and BTZ at concentration gradients ranging from 100 pM to 1 mM and fixed 10  $\mu$ M HEWL concentration. The relative fluorescence intensities normalized to the fluorescence signal of HEWL amyloid fibrils alone (taken as 100%) are presented in Figure 1. As a decrease in fluorescence indicates the ability of compounds to inhibit the amyloid fibrils' formation, we could conclude that all of the studied compounds inhibit HEWL amyloid fibrillization to some extent. The efficiency is affected by the compound's concentration, heterodimerization, and structure.

A concentration gradient of 7-MEOTA resulted in a steady decline of ThT fluorescence intensity starting at 100 nM concentration (Figure 1A, black triangles). Regarding BTZ (Figure 1A, orange circles) and an equimolar mixture of parent molecules (Figure 1A, dark yellow squares), we observed a steep decline of ThT fluorescence intensity starting from ~80  $\mu$ M concentration. Moreover, the efficiency of the equimolar mixture was worse than 7-MEOTA alone, suggesting a competitive binding of parent molecules. At the highest used concentration (1 mM) the fluorescence intensity reached ~15% for 7-MEOTA, ~40% for BTZ, and ~30% for their mixture, relative to the signal observed for untreated HEWL amyloid fibrils. That corresponds to ~85%, ~60%, and 70% inhibitory activity for 7-MEOTA, BTZ, and their mixture, respectively.

On the other hand, data collected for heterodimer HK 1072 (Figure 1B, magenta triangles) showed a steady decline of the ThT fluorescence with increasing compound concentration starting from the picomolar region. At the highest (1 mM) concentration only ~10% fluorescence signal was observed in comparison to fluorescence detected for untreated lysozyme fibrils. That corresponds to ~90% inhibition of HEWL amyloid aggregation. The inhibitory activity of compounds with shorter linker slightly decreased, namely ~80% inhibition for HK 1070 (Figure 1B, green diamonds) and ~75% inhibition for HK 1068 (Figure 1B, red circles), respectively. The heterodimer with the shortest linker, HK 1066 (Figure 1B,

blue squares), inhibited the HEWL amyloid aggregation by roughly 60%.

Overall, the obtained data suggest that the inhibitory activity of parent molecules 7-MEOTA, BTZ, and their mixture without heterodimerization is significantly lower in comparison to that of the heterodimers. Moreover, an effect of linker length on the inhibitory activity of amyloid aggregation of HEWL was observed. The data presented in Figure 1B suggest that elongation of the linker had a positive effect on a compound's capability to suppress amyloid aggregation of HEWL. The highest inhibition was observed for compound HK 1072 with the longest linker, eight carbons long. The gradual decline in inhibitory activity was observed for heterodimers with a shorter linker length. For better quantification of inhibitory properties of studied compounds, the fluorescence intensity values were fitted. The obtained curves were used for calculation of  $IC_{50}$  values (half-maximal inhibitory concentrations of compounds), which are summarized in Table 2. BTZ showed the lowest inhibitory potential, with the highest  $IC_{50}$  value equal to 871  $\mu$ M. The second parent molecule, 7-MEOTA, exhibited better anti-amyloid properties with an  $IC_{50} \approx 67 \mu$ M. Their equimolar mixture had a higher  $IC_{50}$  value than all the

**Table 2.**  $IC_{50}$  Values of 7-MEOTA, BTZ, Their Equimolar Mixture, and HK Compounds Corresponding to Their Ability to Inhibit Amyloid Aggregation of HEWL<sup>a</sup>

compound	$IC_{50}$ [ $\mu$ M]
7-MEOTA	$66.8 \pm 4.4$
BTZ	$871.4 \pm 64.3$
equimolar mixture 7-MEOTA:BTZ	$196.7 \pm 16.5$
HK 1066	$115.6 \pm 11.3$
HK 1068	$48.7 \pm 7.6$
HK 1070	$15.4 \pm 0.9$
HK 1072	$1.6 \pm 0.3$

<sup>a</sup>Data represent the mean value obtained from three independent measurements and an average deviation.

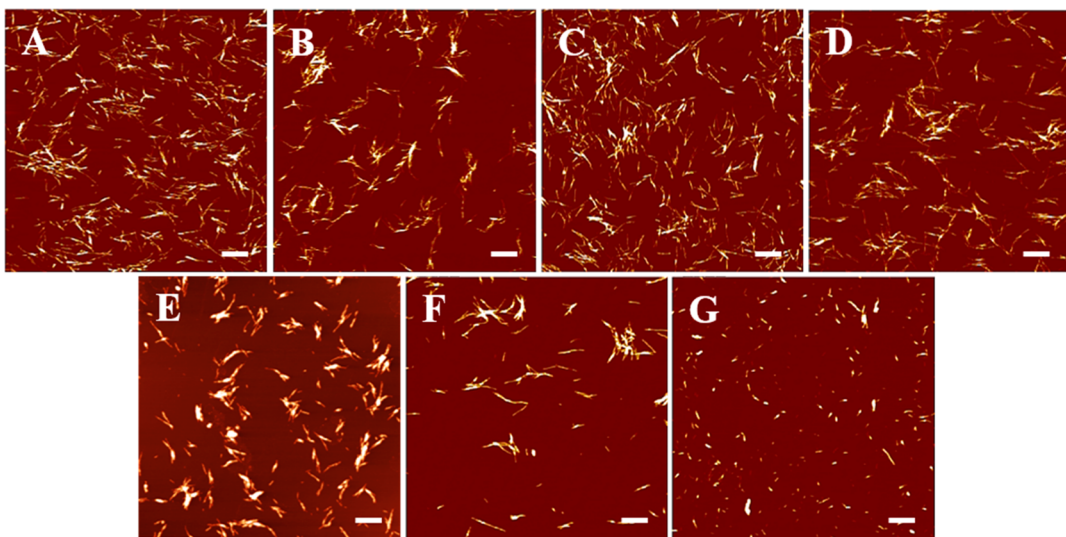


**Figure 2.** AFM images of HEWL fibrils formed alone (A) or in the presence of the studied compounds 7-MEOTA (B), BTZ (C), HK 1066 (D), HK 1068 (E), HK 1070 (F), and HK 1072 (G). The concentration of HEWL was 10  $\mu$ M, and the concentration of added compounds was 500  $\mu$ M. Bars represent 1  $\mu$ m.

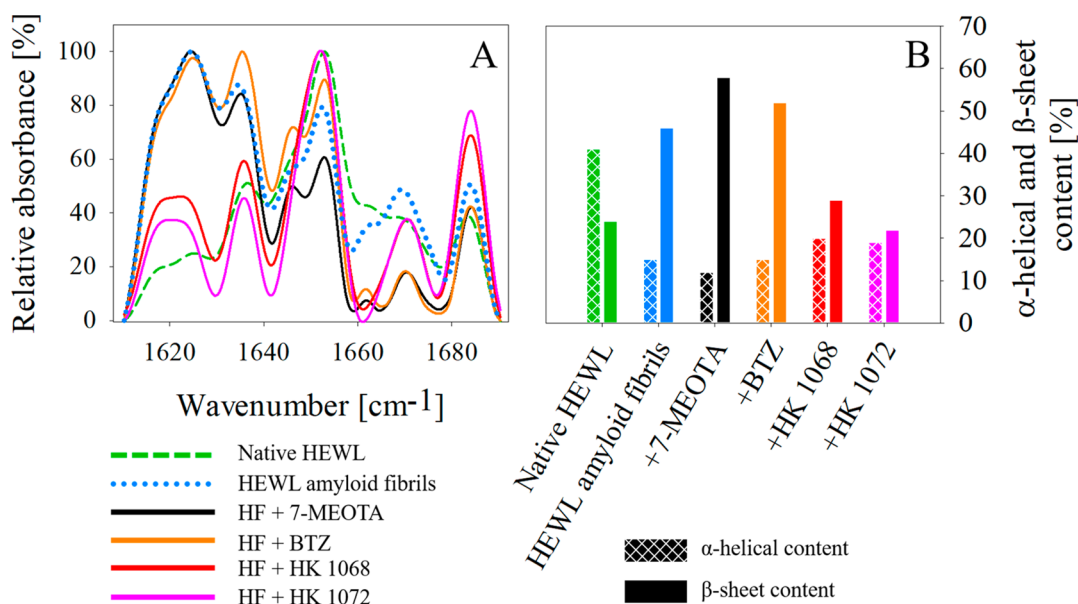


**Figure 3.** (A) ATR FTIR spectra of native 50  $\mu$ M HEWL (green dashed line) and 50  $\mu$ M HEWL amyloid fibrils after fibrillization without added compound (blue dotted line) or in presence of 500  $\mu$ M compound BTZ (orange line), 7-MEOTA (black line), HK 1068 (red line), and HK 1072 (magenta line). (B)  $\alpha$ -Helical (patterned columns) and  $\beta$ -sheet (full-colored columns) content determined for native HEWL, HEWL fibrils, and HEWL fibrillized in presence of compounds BTZ, 7-MEOTA, HK 1068, and HK 1072. The resulting FTIR spectra represent an average of 254 repetitions.

heterodimers, equal to 196.7  $\mu$ M. Importantly, all heterodimers with the exception of HK 1066 were more effective at inhibiting HEWL amyloid aggregation than parent molecules BTZ and 7-MEOTA or their equimolar mixture. Moreover, it was found that, with longer aliphatic linker of heterodimers, the inhibitory efficiency of the compounds increased in correspondence to the decline of their IC<sub>50</sub> values. The most effective compound was the heterodimer HK 1072 with an IC<sub>50</sub>  $\approx$  1.6  $\mu$ M, which is 2 orders of magnitude better than that of BTZ and 1 order enhancement in comparison to 7-MEOTA. The obtained results suggest that both the heterodimerization and linker length are important factors determining a compound's inhibitory ability.

**Morphology of Amyloid Aggregates.** Atomic force microscopy (AFM) was used to visualize morphological changes of HEWL amyloid fibrils forming in the presence of the studied compounds (Figure 2).

For BTZ (Figure 2C) the quantity and morphology of the amyloid fibrils were comparable to those of HEWL amyloid aggregates formed alone, confirming very low inhibitory activity of this compound (Figure 2A). A reduction of the amount of amyloid aggregates was detected for lysozyme fibrillization in the presence of compound 7-MEOTA (Figure 2B). Among the heterodimers, the lowest amount reduction of the amyloid fibrils was observed for HEWL fibrillization in the presence of HK 1066 (Figure 2D) corresponding to its higher IC<sub>50</sub> value. Addition of HK 1068 (Figure 2E) caused

morphology and quantity changes similar to those observed for 7-MEOTA. Considerably fewer aggregates were formed in the presence of compound HK 1070 (Figure 2F), and aggregates formed in the presence of HK 1072 (Figure 2G) in particular appeared much shorter and more amorphous compared to other samples. AFM images of formed aggregates are in a very good correlation with calculated  $IC_{50}$  values and support results obtained from ThT fluorescent assay.

**Secondary Structure Determination: ATR FTIR Spectroscopy.** In order to analyze differences in the content of secondary structure of HEWL amyloid fibrils formed alone and in the presence of studied compounds, samples were examined using ATR FTIR spectroscopy. The FTIR spectra recorded for native and untreated HEWL amyloid fibrils as well as for lysozyme aggregates formed in the presence of parent molecules BTZ, 7-MEOTA, and heterodimers HK 1068 (representing compounds with the short linker) and HK 1072 (compound with the longest linker and the best inhibitory activity) are presented in Figure 3A. The spectra were deconvolved (Figure S1) to calculate the particular protein secondary structures (Table S1). The  $\alpha$ -helical and  $\beta$ -sheet content has been determined for all samples and is presented in Figure 3B.

The absorption spectrum of native HEWL in the amide I region (Figure 3A, green dashed line) shows wide bands at 1653 and 1661  $\text{cm}^{-1}$  corresponding to ~41%  $\alpha$ -helical content (Figure 3B, green patterned column), which is in agreement with other studies.<sup>23</sup> Bands at 1625 and 1636  $\text{cm}^{-1}$  represent ~24%  $\beta$ -sheet content (Figure 3B, green full-color column). In contrast, HEWL amyloid fibrils formed alone (Figure 3A, blue dotted line) have bands at 1624 and 1636  $\text{cm}^{-1}$ , indicating a significant increase in  $\beta$ -sheet content, characteristic for HEWL amyloid fibrils.<sup>4</sup> Calculated  $\beta$ -sheet content for HEWL amyloid fibrils was ~46% (Figure 3B, blue full-color column). This significant increase was mainly at the expense of lower  $\alpha$ -helical content in HEWL amyloid fibrils (~15%) (Figure 3B, blue patterned column).

Addition of studied parent molecules BTZ (Figure 3A, orange line) and 7-MEOTA (Figure 3A, black line) led to slight changes in the spectra compared to the ones detected for HEWL fibrils; interestingly, the  $\beta$ -sheet content was higher (58% for 7-MEOTA and 52% for BTZ) (Figure 3B, black and orange full-color columns) than we observed for lysozyme fibrils alone (46%). An effect of HK 1068 and HK 1072 heterodimers on the secondary structure content of HEWL amyloid aggregates was significantly different. Bands at 1623 and 1636  $\text{cm}^{-1}$  (Figure 3A, red and magenta lines) related to the  $\beta$ -sheet secondary structure were still observed, however at much lower intensity. The spectral deconvolution (Figure 3B, red and magenta full-colored columns) determined ~29% and ~22%  $\beta$ -sheet content for HK 1068 and HK 1072, respectively. Interestingly, the observed decrease in  $\beta$ -sheet content in comparison to HEWL amyloid fibrils prepared alone was mostly at the cost of an extensive increase of random coil (~10%),  $\beta$ -turn content (~4–10%), and a minor increase of the  $\alpha$ -helical structures (~5%). These results indicate that the heterodimers HK 1068 and HK 1072 were able to prevent the formation of cross- $\beta$  structures unique for amyloid fibrils, while also conserving part of  $\alpha$ -helical structure. The content of secondary structures is shown in the Supporting Information (SI) (Figure S1 and Table S1).

**Docking Results.** In docking simulation, a  $40 \times 45 \times 50 \text{ \AA}^3$  box with the center of mass at  $(-1.74, 0.06, -9.33) \text{ \AA}$  was

used. The binding location of six studied compounds in HEWL is shown in Figure 4. All compounds have almost the

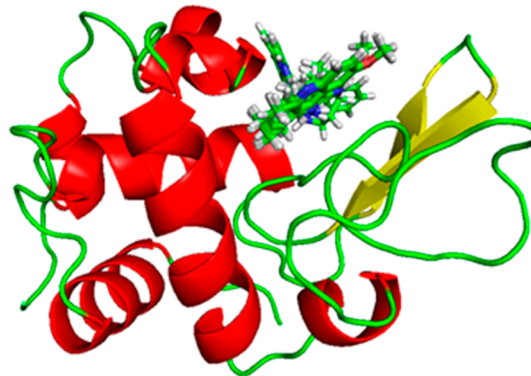


Figure 4. Binding site of six studied compounds in HEWL.

same binding position, with five common residues: Trp63, Asn59, Asp52, Gln57, and Ala107. More detailed information about the ligands in the binding pocket is summarized in Table S2 and Figure S2.

Contact networks determined for the studied compounds in the best docking mode are shown in Figures S3 and S4. Except for the HK 1070 compound, which forms one hydrogen bond (HB) with Asn46, no other compounds develop hydrogen bonds with HEWL, indicating that HBs do not prevail in the binding affinity of HK compounds. The number of nonbonded contacts (NBCs) is 7, 9, 13, 14, 12, and 11 for BTZ, 7-MEOTA, and HK 1066, HK 1068, HK 1070, and HK 1072 heterodimers, respectively (Table S3, Figures S3 and S4). The HK 1066 compound has the highest number of NBCs (14) and, therefore, the highest binding affinity— $\Delta E_{\text{bind}} = -8.7 \text{ kcal}\cdot\text{mol}^{-1}$ . The BTZ compound with the fewest number of NBCs has the worst binding affinity,  $\Delta E_{\text{bind}} = -5.7 \text{ kcal}\cdot\text{mol}^{-1}$ . Thus, the NBC network is superior to the HB network in terms of the binding affinity of HK compounds. The binding affinity of all compounds is also summarized in Table S3. The correlation between  $\Delta E_{\text{bind}}$  and  $IC_{50}$  values is high with the correlation level,  $R = 0.78$  (Figure S5).

**MM-PBSA Result: Binding Free Energy.** Because results from molecular docking are not sufficiently reliable, we estimated the binding free energy using molecular dynamics (MD) simulation and the MM-PBSA method. For each receptor–ligand complex, we performed five independent 100 ns MD runs starting from the same starting configuration, obtained in the best docking mode (Figure 4), but with different random seed numbers to create different initial velocities. In order to estimate the equilibration time  $\tau_{\text{eq}}$ , we controlled the time dependence of RMSD assuming that equilibrium was reached if this dependence gets saturated. Apparently,  $\tau_{\text{eq}}$  depends on the compound and the trajectory ranging from 40 to 60 ns (Figure S6). Snapshots collected at equilibrium represented by arrows in Figure S6 were used to compute  $\Delta G_{\text{bind}}$  (eq 1). The obtained data are presented in Table 3.

The lowest  $\Delta G_{\text{bind}}$  ( $-32.5 \pm 5.2 \text{ kcal}\cdot\text{mol}^{-1}$ ) was obtained for the HK 1072 compound, which is in correlation with the *in vitro* experiments, showing that this compound has the best inhibitory effect and the lowest  $IC_{50}$  value. The binding free energy calculated by the MM-PBSA method strongly correlates with the number of carbon atoms of the linker (Figure 5), as

**Table 3.** Binding Free Energy ( $\text{kcal}\cdot\text{mol}^{-1}$ ) Obtained by the MM-PBSA Method<sup>a</sup>

ligand	$\Delta E_{\text{elec}}$	$\Delta E_{\text{vdW}}$	$\Delta G_{\text{PB}}$	$\Delta G_{\text{SA}}$	$-TS$	$\Delta G_{\text{bind}}$	$\Delta G_{\text{exp}}$
7-MEOTA	$-25.1 \pm 2.9$	$-21.2 \pm 2.0$	$11.5 \pm 3.6$	$-7.1 \pm 0.4$	$24.3 \pm 2.9$	$-17.6 \pm 5.2$	$-5.7$
BTZ	$-13.6 \pm 2.8$	$-14.8 \pm 2.2$	$4.3 \pm 1.7$	$-6.8 \pm 0.2$	$23.3 \pm 2.1$	$-7.4 \pm 2.4$	$-4.2$
HK 1066	$-20.1 \pm 7.4$	$-20.7 \pm 3.7$	$6.2 \pm 4.7$	$-7.4 \pm 0.4$	$26.2 \pm 2.9$	$-15.8 \pm 3.2$	$-5.4$
HK 1068	$-14.2 \pm 1.1$	$-28.4 \pm 6.1$	$7.7 \pm 2.1$	$-7.5 \pm 0.4$	$23.8 \pm 4.1$	$-18.7 \pm 4.9$	$-5.7$
HK 1070	$-23.5 \pm 9.6$	$-25.1 \pm 8.0$	$6.4 \pm 1.0$	$-7.1 \pm 0.4$	$22.1 \pm 3.3$	$-27.2 \pm 4.7$	$-6.5$
HK 1072	$-24.3 \pm 5.4$	$-31.2 \pm 3.5$	$10.3 \pm 2.1$	$-6.4 \pm 0.4$	$19.2 \pm 3.0$	$-32.5 \pm 5.2$	$-7.9$

<sup>a</sup>The experimental binding free energy was estimated using the equation  $\Delta G_{\text{exp}} = RT \ln(\text{IC}_{50})$ , where  $T = 300 \text{ K}$  and the gas constant  $R = 1.987 \times 10^{-3} \text{ kcal K}^{-1} \text{ mol}^{-1}$ .

well as with  $\text{IC}_{50}$  values (Figure S7) and  $\Delta G_{\text{exp}}$  (Figure S8). This means that the addition of the carbon linker leads to a stronger interaction between compounds and HEWL.

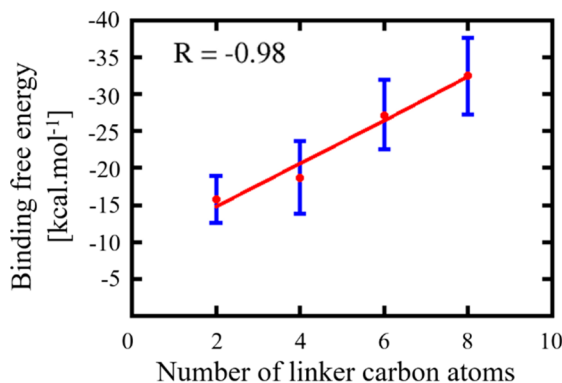


**Figure 5.** Correlation between binding free energy (MM-PBSA) and the number of linker carbon atoms. Error bars represent standard deviation.

To shed more light on the binding mechanism, HK compounds were divided into three structural blocks (Figure 6). The first block is a linker region, which consists of 2 (HK 1066)

1066), 4 (HK 1068), 6 (HK 1070), or 8 (HK 1072) carbon atoms. Therefore, block 1 has 6, 12, 18, and 24 atoms for HK 1066, HK 1068, HK 1070, and HK 1072, respectively. Block 2 of 7-MEOTA has 33 atoms and block 3 of BTZ has 16 atoms.

Contribution of block 1 varies and depends on the number of carbon atoms in the linker (Table 4). The van der Waals

**Table 4. Decomposition of the Interaction Energy ( $\text{kcal}\cdot\text{mol}^{-1}$ ) into Three Blocks**

ligand	block 1		block 2		block 3	
	$\Delta E_{\text{elec}}$	$\Delta E_{\text{vdW}}$	$\Delta E_{\text{elec}}$	$\Delta E_{\text{vdW}}$	$\Delta E_{\text{elec}}$	$\Delta E_{\text{vdW}}$
HK 1066	-8.0	-1.8	-3.7	-15.3	-8.3	-3.6
HK 1068	-4.9	-4.5	-2.1	-17.4	-7.2	-6.6
HK 1070	-7.2	-4.9	-5.5	-13.9	-10.8	-6.3
HK 1072	-11.9	-9.3	-4.7	-15.6	-6.1	-5.4

(vdW) interaction of block 1 with the HEWL molecule greatly increases from  $-1.8$  to  $-10.0 \text{ kcal}\cdot\text{mol}^{-1}$ , whereas the contributions of block 2 and block 3 are almost equal. The contribution of block 2 to the vdW interaction is more important than that of the other two blocks since it has more atoms (33 atoms). In general, block 1 contributes to the vdW interactions less than block 2; however, the overall trend is that the higher number of linker carbons, the stronger binding of

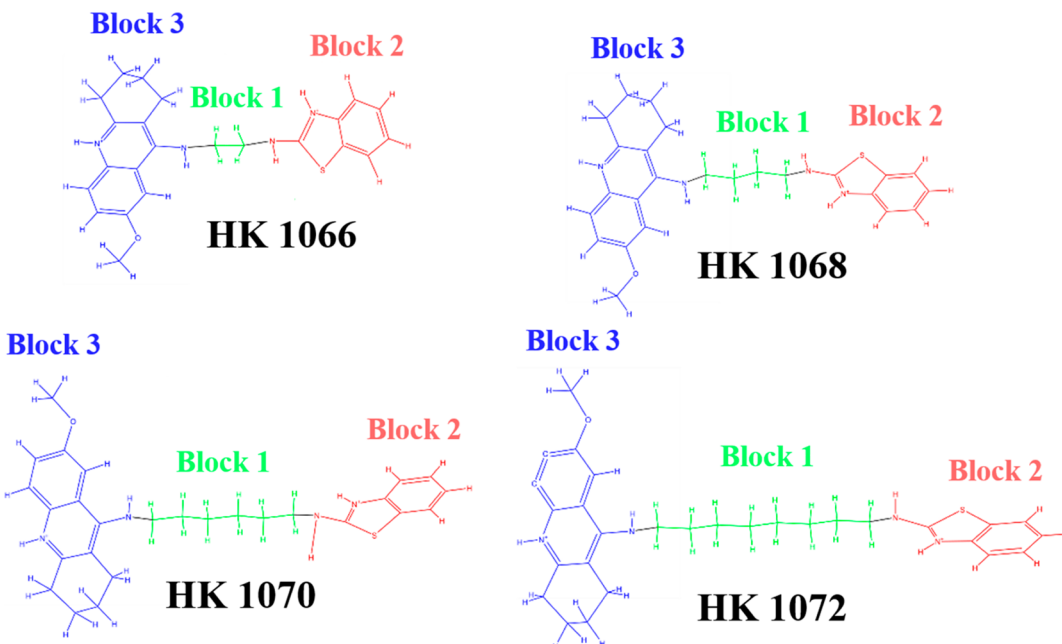


**Figure 6.** Three structural blocks of HK compounds. Block 1 represents aliphatic linker (green), block 2 corresponds to the first parent molecule BTZ (red), and block 3 is the second parent molecule 7-MEOTA (blue).

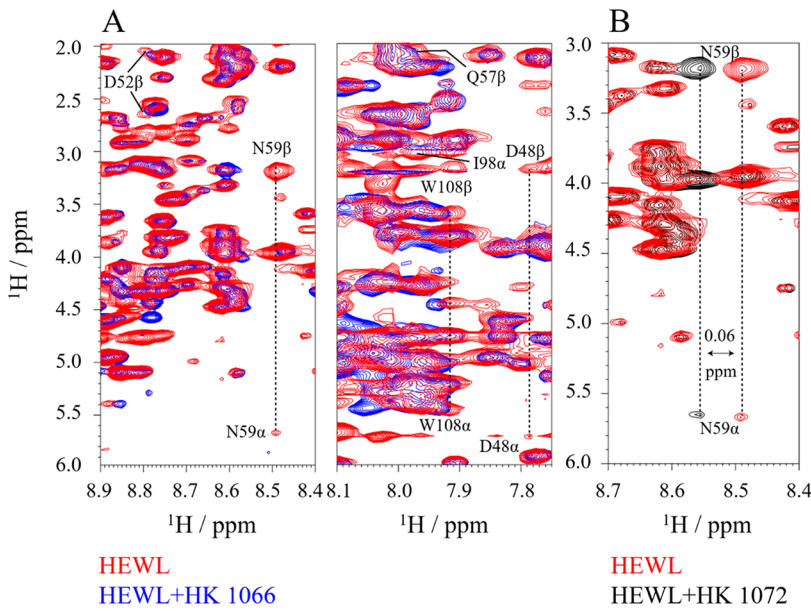


**Figure 7.** 2D NOESY spectra of free HEWL (red) and in the presence of (A) HK 1066 (blue) or (B) HK 1072 (black). The superimposed spectra confirm the residue-specific chemical shift perturbations (CSPs). CSPs were obtained for several residues that are involved in binding with the ligands, which were in accordance with the molecular docking.

the ligand to the HEWL molecule. Regarding electrostatic interactions, we observed fluctuations within an error, which correlates well considering the structures of parent molecules are identical and their binding positions are roughly the same.

**Binding Epitope of HEWL: Small Molecule Interaction.** Two-dimensional homonuclear NOESY experiment was done to elucidate the structural perturbation of HEWL in the presence of HK 1066 and HK 1072 at an equimolar ratio. Figure 7 depicts the superimposed spectra of HEWL in the absence and presence of ligands (HK 1066 and HK 1072). After careful investigation, several chemical shift perturbations (CSPs) were observed in both cases, but HK 1066 showed peak broadening effect against several amino acid residues such as Asp48, Asp52, Asn59, and Trp108 (Figure 7A). The same effect was also observed for  $\text{CaH}$  of Ile98 and  $\text{C}\beta\text{Hs}$  of Gln57. On the contrary, in the presence of HK 1072 residues, Asn59 and Trp108 (data not shown) showed a downfield CSP of  $\sim 0.06$  and  $0.02$  ppm, respectively (Figure 7B). Other amino acid residues responsible for binding to HK 1072 as evidenced from the molecular docking analysis remained unchanged in the NOESY spectrum.

Additionally, the remarkable CSPs were observed for the indole ( $\text{NeH}$ ) ring protons of Trp62 and Trp111 of HEWL in the presence of the ligands HK 1066 and HK 1072 (Figure 8). Trp62 showed  $\sim 0.13$  and  $0.08$  ppm downfield CSP for HK 1066 and HK 1072, respectively, while Trp111 showed  $\sim 0.07$  and  $0.04$  upfield CSPs after addition of equimolar concentrations of HK 1066 (Figure 8A) and HK 1072 (Figure 8B), respectively. It is noteworthy that the Trp63 and Trp108 of HEWL have been shown to interact with the HK compounds in molecular docking analysis, but these residues showed minimal (in presence of HK 1066) to no (in presence of HK 1072) CSPs in the NOESY spectrum. Surprisingly, their neighboring residues, such as Trp62 and Trp111, showed significant chemical shift perturbation upon addition of the equimolar concentration of the HK ligands. Generally, aromatic–aromatic interactions along with hydrophobic

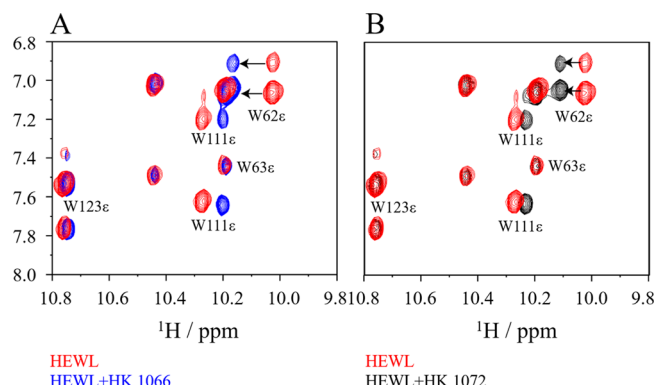


**Figure 8.** Chemical shift perturbation of indole ( $\text{NeH}$ ) ring proton belonging to tryptophan residues of HEWL in the presence of either HK 1066 (A) or HK 1072 (B), indicating that these moieties play a crucial role during binding of the ligand molecules.

stacking plays a crucial role to halt the amyloid aggregation of HEWL molecules.<sup>24</sup>

Next, saturation transfer difference (STD) NMR was performed to define the epitope of the ligands, binding to HEWL. In this study, the ligand to HEWL concentration was kept at 300:1 ratio to enhance the “STD amplification factor”.<sup>25,26</sup> Careful analysis of the data suggests that both HK compounds interact with HEWL as evidenced by strong STD peaks of the  $-\text{CH}_2/-\text{CH}_3$  groups along with comparatively low signals from aromatic ring protons (Figure 9). Interestingly, the acyl chain protons (linker protons) of HK 1072 have shown comparatively stronger interaction than those associated with HK 1066 (as shown in inset), correlating well with the previous observations like ThT assays and MD simulations.

One of the generally accepted therapeutic strategies for amyloidoses is the inhibition of amyloid aggregation of peptides and polypeptides and/or removal of insoluble amyloid fibrils from the affected tissue. There are many reports documenting a great potential of small molecules to

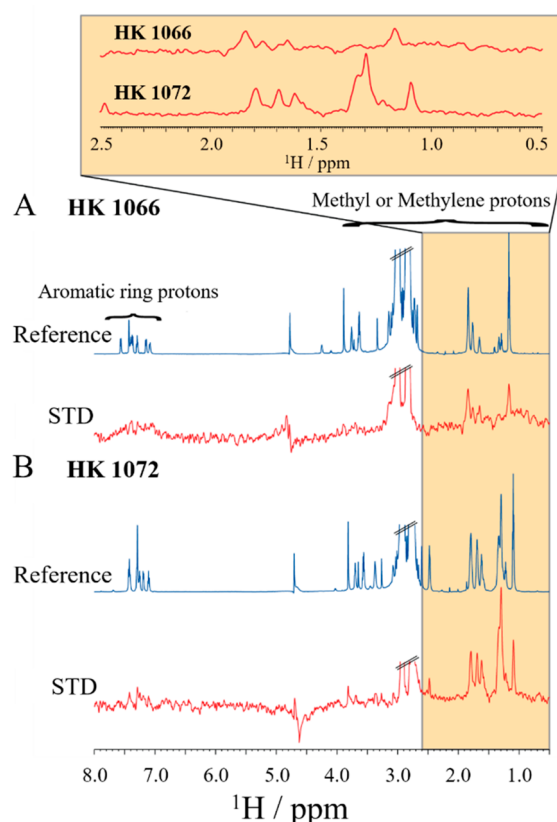


**Figure 9.** 1D STD NMR analysis of free and bound HK 1066 and HK 1072 in the presence of HEWL. The aliphatic ( $\text{CH}_2/\text{CH}_3$ ) and aromatic ring protons of HK compounds are in close proximity to the HEWL; however, relatively stronger STD signal was observed for methylene protons of HK 1072 in comparison to HK 1066.

interfere with amyloid fibrillation of peptides and polypeptides leading to decreasing of the amount of the amyloid aggregates. It was found that small molecules interfere with amyloid fibrillation through interaction with various amyloidogenic species produced in the aggregation process, and several mechanisms of action were suggested concerning their anti-amyloid activity.<sup>7,10,29–33,12–17,27,28</sup> Re et al. suggested that intercalation of a small molecule within grooves created by  $\beta$ -sheets in both soluble oligomeric forms as well as in the mature amyloid fibrils leads to inhibitory activity.<sup>27</sup> Another proposed mode of action rests on the binding of a small molecule into the hydrophobic region of peptides and polypeptides and interaction with neighboring amyloidogenic residues, subsequently leading to inhibition of self-assembly process and amyloid polymerization.<sup>28</sup> In 2014, Takai et al. discussed the effects of amino acids on the amyloid aggregation of lysozyme showing that the presence of cysteine significantly contributes to the inhibition of amyloid formation by noncovalent interaction between the thiol group of cysteine and the core sequence of lysozyme.<sup>29</sup> Ascorbic acid inhibited amyloid fibrillation of lysozyme. Proposed mechanism of action suggests binding to the aggregation-prone region of lysozyme, stabilizing its partially unfolded state, and thus preventing further conformational changes leading to fibrillization.<sup>30</sup>

Structure–activity relationship study of several small molecules toward the amyloid aggregation of peptides and polypeptides has been performed. It was found that presence

of aromatic structures in small molecules represents important factor for anti-amyloid properties of many compounds.<sup>7,31–33</sup> To improve the effectivity of small compounds to influence amyloid aggregation the accumulation of cyclic structures into one multiple cyclic molecule was suggested. Lieu et al. demonstrated that the formation of lysozyme amyloid fibrils was markedly inhibited by the presence of rifampicin and its analogue *p*-benzoquinone in a dose-dependent fashion.<sup>32</sup> Phenolic and polyphenolic compounds have been reported to inhibit the amyloid formation of peptides and polypeptides.<sup>17</sup> Catechol and hydroquinone inhibited lysozyme amyloid aggregation by covalent binding to the peptide chain, forming quinoproteins.<sup>31</sup> A number of acridine derivatives have shown the ability to inhibit lysozyme amyloid aggregation.<sup>33</sup> Many other small polycyclic compounds have been tested and acknowledged as potential drug candidate prototypes for the treatment of amyloidoses.<sup>10</sup>

Based on this knowledge, we decided to study the effect of two compounds 7-MEOTA and BTZ on the amyloid aggregation of HEWL. Both molecules consist of two (BTZ) or three (7-MEOTA) cyclic structures. Moreover, 7-MEOTA belongs to tacrine analogues for which the anti-amyloid activities have already been reported.<sup>27,34,35</sup> We have found that these molecules were able to affect lysozyme amyloid fibrillation to some extent. The 7-MEOTA is quite effective with an  $\text{IC}_{50}$  value of  $66.8 \mu\text{M}$ . Surprisingly, the efficiency of BTZ to inhibit HEWL fibrillization is significantly lower corresponding to an  $\text{IC}_{50}$  value of  $871.4 \mu\text{M}$ . We suggest that the reason behind this difference is lack of vdW interaction leading to lower total affinity. Overall, our data support finding that small molecules containing multiple cycles are able to interfere with amyloid aggregation.

Currently, there is a new strategy to improve the inhibitory efficiency of small compounds based on combining multiple cyclic functional molecules into one heterodimeric compound. The aim is an enhancement of anti-aggregation capabilities due to the synergy of two or more active structures.<sup>20,22</sup> Besides the aromatic multicycles, a linker connecting two functional molecules has proven to be another promising structure to optimize and modulate the effects of heterodimers. The relationship between inhibitory potency of heterodimers designed against amyloid aggregation, the structure of functional molecules and properties of the linker has been already reported. In 2007, Reinke and Gestwicki defined a narrow region of optimal linker length and flexibility in case of curcumin derivatives. Both these parameters strongly influenced the potency of studied compounds against amyloid-beta aggregation.<sup>8</sup> In 2018, Ulicna et al. described a series of tacrine–coumarine heterodimers effective against amyloid aggregation of lysozyme. These derivatives differed in linker length as well as its structure. Compounds containing plain aliphatic linker have shown the greatest inhibition efficiency. It has been demonstrated that linker longer than  $\sim 9 \text{ \AA}$  inhibited the formation of lysozyme amyloid fibrils at lower potency, suggesting an upper limit to the effective length of linker region.<sup>28</sup>

Our results obtained for the studied heterodimers consisting of 7-MEOTA and BTZ functional molecules connected by aliphatic linker point to their significantly higher inhibitory activity compared to separate parent molecules. The  $\text{IC}_{50}$  values of studied heterodimers were lower (HK 1068,  $48.7 \mu\text{M}$ ; HK 1070,  $15.4 \mu\text{M}$ ; HK 1072,  $1.6 \mu\text{M}$ ) than the  $\text{IC}_{50}$  of functional molecules (BTZ,  $871.4 \mu\text{M}$ ; 7-MEOTA,  $66.8 \mu\text{M}$ )

with exception of derivative HK 1066 ( $115.6 \mu\text{M}$ ). These results indicate that heterodimerization improves the anti-amyloid properties of the parent molecules. The detailed analysis of the obtained results suggests that elongating the linker region increased the efficiency of the heterodimers. Considering the functional molecules in heterodimers were identical, we suggest that the length of the linker region plays an important role in compounds anti-amyloid potency.

The data obtained using ThT fluorescence assay were confirmed by microscopy, namely by AFM. Negligible changes in the amount and morphology of amyloid fibrils were observed after treatment of HEWL fibrillization with BTZ alone. Moderate inhibitory efficiency was detected for the second parent molecule 7-MEOTA. The effect of heterodimerization and elongation of the linker was evident as changes in the amount and also morphology got more apparent in the presence of the heterodimers HK 1070 and HK 1072.

ATR FTIR data supported the previous results since HEWL fibrillization in the presence of parent molecules, BTZ and 7-MEOTA, leads to subtle changes in the protein secondary structure and notable  $\beta$ -sheet content increase. On the other hand, the inhibitory activity of the heterodimers HK 1068 and HK 1072 resulted in an extensive decrease in the  $\beta$ -sheet content and minor preservation of the  $\alpha$ -helical structure in produced HEWL amyloid fibrils.

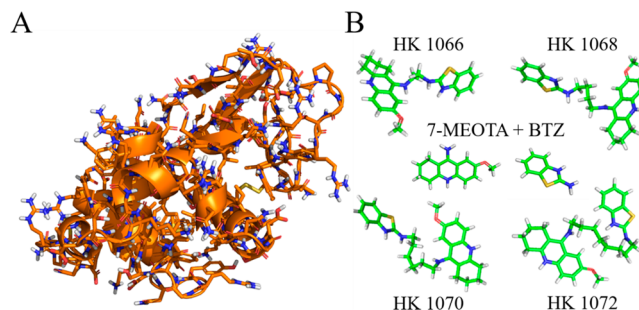
*In silico* methods were used to better understand the relationship between the structure of studied compounds and their inhibitory effect. Calculations indicate that the binding site of all studied compounds is very similar. Overall, the NBC network was better than HB network in the characterization of binding affinity of compounds. In all cases, compounds made NBCs with HEWL residues Asp52, Gln57, Asn59, Trp63, and Ala107. It is well established in the literature that lysozyme region 49–109 is of particular significance in the process of fibril formation. This region, including  $\beta$ -domain and C-helix, is considered the most amyloidogenic one of full-length HEWL.<sup>36,37</sup> Canet et al. have demonstrated the ability of  $\beta$ -domain and the adjacent C-helix to unfold in a locally cooperative manner.<sup>38</sup> Moreover, C-helix (98–109) has the lowest propensity of HEWL helices to form  $\alpha$ -helical structure, which is likely to be a significant factor in the formation of amyloid fibrils rich in  $\beta$ -sheet content.<sup>37</sup> Although BTZ interacts with all residues mentioned above, docking study revealed its lowest binding affinity to HEWL. Upon further examination of NBC network for all studied compounds (Table S2) it should be noted that BTZ, in comparison to the rest of compounds including 7-MEOTA, lacks interaction with the region 44–48. Despite the fact that this region is not considered a major amyloidogenic contributor, interaction with this region enhances the binding affinity of small molecules to HEWL, as well as their anti-amyloid effects. Therefore, 7-MEOTA's ability to interact with these residues explains its higher affinity toward HEWL molecule and preservation of this property after the heterodimerization is possibly one of the key factors associated with the effective inhibition of HEWL amyloid aggregation by designed heterodimers.

MM-PBSA calculations support results obtained from the docking studies and indicate that the vdW interactions predominate over electrostatic interactions in compounds binding to HEWL. To shed more light into the binding mechanism, the structure of heterodimers was divided into

three blocks. Considering the structure of blocks 2 and 3 is identical for every heterodimer, their contribution to binding affinity is also identical within an error. Thus, the decisive factor that explains the variance in binding affinity of heterodimers (Table 3) and their anti-amyloid properties represented by  $\text{IC}_{50}$  values (Table 2) is block 1, the linker region (Table 4).

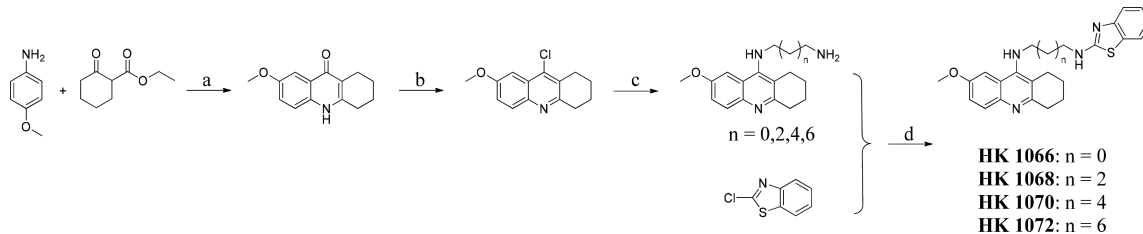
Regarding the higher  $\text{IC}_{50}$  value of 7-MEOTA and BTZ equimolar mixture, based on the docking simulation results we concluded that 7-MEOTA and BTZ compete for the identical binding site, therefore its efficiency is worse than individual 7-MEOTA. We propose a similar explanation for the compound HK 1066, which has the shortest linker among the heterodimers. 7-MEOTA (block 3) of the HK 1066 binds to its high-affinity site, while BTZ (block 2) does not and presumably competes with 7-MEOTA (block 3), which explains lower affinity compared to 7-MEOTA alone. Moreover, we observed that after heterodimerization BTZ (block 2) occupies a new binding location in close proximity to residues Phe34 and Glu35. The obtained results show a big increase in absolute binding free energy with elongating linker region. We assume that longer linker region allows BTZ (block 2) to approach the new binding site more conveniently, which is not possible especially in the case of HK 1066.

The binding free energy estimated by MM-PBSA and the number of carbon atoms in linker structure of heterodimers correlate very well (Figure 6). These subtle changes in binding free energy lead to greater stabilization of HEWL structure, preventing the creation of early amyloidogenic species. However, the sharp decline in  $\text{IC}_{50}$  values might not be the consequence of binding affinity alone. As demonstrated in the docking results, studied heterodimers interact with region 49–109 considered as most important in the formation of amyloid fibrils. NBC network representation (Figure S4) and STD NMR (Figure 10) results suggest that the linker region



**Figure 10.** 3D structures of studied receptor protein and compounds at pH 2.7. (A) The structure of HEWL. The side chain hydrogen and nitrogen atoms are colored in white and blue, respectively; disulfide bonds are colored in yellow. (B) The structures of parent molecules 7-MEOTA, BTZ, and synthesized heterodimers HK 1066, HK 1068, HK 1070, and HK 1072.

interacts with residues in close proximity to the C-helix domain (residues 98–109). The presence of heterodimer in binding site possibly blocks the interaction between the  $\beta$ -domain and the C-helix, halting the formation of partially unordered regions essential for cross- $\beta$  structure. Elongation of the linker ultimately enhances a compound's ability to prevent this interaction by greater steric obstruction.

**Scheme 1.** Synthesis of HK Compounds: HK 1066, HK 1068, HK 1070, and HK 1072<sup>a</sup>

<sup>a</sup>Reagents and conditions: (a) toluene, H<sub>2</sub>O, diphenyl ether, EtOH, Dean–Stark trap; (b) POCl<sub>3</sub>; (c)  $\alpha,\omega$ -diaminoalkane, phenol; (d) DIPEA, DMF.

## CONCLUSION

Combining multiple functional moieties while conserving their fundamental properties in one molecule with enhanced activity is a novel approach to target amyloidoses. In this study, we investigated the activity of 7-MEOTA–BTZ heterodimers, HK compounds, toward amyloid aggregation of lysozyme. Using several *in vitro* and *in silico* techniques, we showed that heterodimerization has a substantial impact on the effectiveness of the compounds. As a result, HK compounds exhibited a much higher ability to inhibit amyloid aggregation of HEWL in comparison to their parent molecules. Despite the fact that, according to *in silico* calculations, individual 7-MEOTA and BTZ molecules occupy the same binding site, the best HK compounds have more than double the binding affinity to lysozyme. In the case of heterodimers, we assume that BTZ (block 2), which has lower affinity than 7-MEOTA (block 3), presumably binds to another location instead of competing with 7-MEOTA. When certain conditions are met, namely the linker length, inhibitory efficacy improvement was observed. We suggest that this dependency is connected to the interaction of the aliphatic linker with residues in the C-helix sequence (98–109) of the HEWL molecule. We demonstrated that elongation of the linker leads to the higher affinity of HK compounds as the vdW interaction of the linker region increases and BTZ binds more effectively. We also suggest that their anti-amyloid activity is related to the steric obstruction between the  $\beta$ -sheet-rich and C-helix regions of the HEWL molecule, which are considered essential for the formation of the amyloid structures.

The obtained results represent an important contribution for the recent rational design of potential lead small molecules with anti-amyloid properties, and the studied heterodimers are prospective candidates for the treatment of systemic lysozyme amyloidosis and other amyloid-related diseases.

## MATERIAL AND METHODS

**Chemicals.** HEWL (L6876, activity ~40 000 units·mg<sup>-1</sup> protein, E.C. number 3.2.1.17), thioflavin T (ThT), dimethyl sulfoxide (DMSO), glycine, NaCl, and Dulbecco's Modified Eagle Medium (DMEM) were purchased from the Sigma-Aldrich Chemical Co. (St. Louis, MO, USA). SH-SY5Y human neuroblastoma cell line was purchased from German Collection of Microorganisms and Cell Culture, DSMZ (Braunschweig, Germany), and WST-1 Cell Proliferation Assay Kit (WST-1) from Roche Diagnostics GmbH (Mannheim, Germany). 4,4-Dimethyl-4-silapentane-5-sulfonate sodium salt (DSS), *d*<sub>6</sub>-DMSO, and D<sub>2</sub>O were obtained from Cambridge Isotope Laboratories, Inc. (Tewksbury, MA, USA). Citrate was purchased from Merck Millipore (Burlington, MA, USA), and disodium hydrogen phosphate was purchased from HiMedia Laboratories Pvt. Ltd. (Mumbai, India). All chemicals were of analytical reagent grade. Studied 7-MEOTA–2-aminobenzothiazole

(BTZ) heterodimers (HK compounds) (Table 1) were synthesized at the Department of Chemistry, Faculty of Science, University of Hradec Kralove, Hradec Kralove, Czech Republic. All chemical reagents used for synthesis were purchased from Sigma-Aldrich. Solvents for synthesis were obtained from Penta Chemicals (Prague, Czech Republic).

**Synthesis of HK Compounds.** Novel 7-MEOTA-BTZ heterodimers (HK 1066, HK 1068, HK 1070, and HK 1072) were obtained as depicted in Scheme 1. 7-Methoxy-1,3,4,10-tetrahydroacridin-9(2H)-one, 9-chloro-7-methoxy-1,2,3,4-tetrahydroacridine, and *N*-(7-methoxy-1,2,3,4-tetrahydroacridin-9-yl)alkanediamines were synthesized according to the procedures already reported in the literature.<sup>39,40</sup> Subsequent coupling with 2-chloro-1,3-benzothiazole in the presence of *N,N*-diisopropylethylamine (DIPEA) in dimethylformamide (DMF) at 110 °C for 2 h provided target compounds in moderate yields. All new hybrids were finally structurally characterized in the form of hydrochloride salts by their analytical and spectroscopic data.

Round-bottom flask with 2-chlorobenzothiazole (1 equiv) was purged with argon and treated with DMF (5 mL). Thereafter, *N,N*-diisopropylethylamine (2 equiv) was added to the mixture. Finally, appropriate  $\alpha,\omega$ -diaminotacrine derivative (1 equiv) dissolved in a small amount of DMF was added to the flask. Formed solution was then heated to 110 °C and stirred for 2 h. After cooling to room temperature, the mixture was dissolved in CH<sub>2</sub>Cl<sub>2</sub> (3 × 100 mL) and extracted with water (100 mL). Collected organic layers were dried over Na<sub>2</sub>SO<sub>4</sub>, filtered, and evaporated to give crude product. Purification by column chromatography using ethyl acetate/MeOH/26% aqueous ammonia solution (60/1/0.2) as eluent provided a pure base. Obtained base was dissolved in MeOH and saturated with gaseous HCl. Solvent removal afforded an oily residue which was subsequently washed with acetonitrile to give the final product in the form of hydrochloride salt.

The course of the reactions was monitored by thin-layer chromatography on aluminum plates precoated with silica gel 60 F254 (Merck, Czech Republic) and then visualized by UV 254. Melting points were determined on a melting point apparatus M-565 (Büchi, Switzerland) and are uncorrected. Uncalibrated purity was ascertained by LC-UV (at the wavelength of 254 nm) using a reverse phase C18 chromatographic column. All the biologically tested compounds exhibited purity 99% at a wavelength 254 nm. NMR spectra of target compounds were recorded on Varian S500 spectrometer (operating at 500 MHz for <sup>1</sup>H and 126 MHz for <sup>13</sup>C; Varian Corp., Palo Alto, CA, USA). Chemical shifts are reported in parts per million (ppm). Spin multiplicities are given as s (singlet), d (doublet), dd (doublet of doublets), t (triplet), p (pentaplet), or m (multiplet). The coupling constants (*J*) are reported in hertz (Hz). High-resolution mass spectra (HRMS) were determined by Q Exactive Plus hybrid quadrupole-orbitrap spectrometer.

***N*<sup>2</sup>-(1,3-Benzothiazol-2-yl)-*N*<sup>1</sup>-(7-methoxy-1,2,3,4-tetrahydroacridin-9-yl)ethane-1,2-diamine Hydrochloride (HK 1066).** Yield 38%; mp 190.4–191.6 °C; purity 99%. <sup>1</sup>H NMR (500 MHz, methanol-*d*<sub>4</sub>):  $\delta$  7.73 (d, *J* = 8.0 Hz, 1H), 7.68 (d, *J* = 2.6 Hz, 1H), 7.62 (d, *J* = 9.2 Hz, 1H), 7.51–7.44 (m, 2H), 7.37–7.32 (m, 2H), 4.31 (t, *J* = 5.7 Hz, 2H), 4.00 (t, *J* = 5.7 Hz, 2H), 3.96 (s, 3H), 3.05 (t, *J* = 6.3 Hz, 2H), 2.86 (t, *J* = 6.2 Hz, 2H), 2.00–1.89 (m, 4H).

<sup>13</sup>C NMR (126 MHz, DMSO-*d*<sub>6</sub>):  $\delta$  167.01, 163.15, 156.84, 155.33, 150.34, 132.48, 126.79, 124.05, 123.22, 122.31, 120.84, 118.06, 112.37, 103.43, 56.36, 45.55, 28.04, 25.43, 24.81, 21.89, 20.28. HRMS: [M+H]<sup>+</sup> 405.1742 (calculated for [C<sub>23</sub>H<sub>25</sub>N<sub>4</sub>OS]<sup>+</sup>: 405.1704).

**N<sup>4</sup>-(1,3-Benzothiazol-2-yl)-N<sup>1</sup>-(7-methoxy-1,2,3,4-tetrahydroacridin-9-yl)butane-1,4-diamine Hydrochloride (HK 1068).** Yield 16%; mp 174.9–175.1 °C; purity 99%. <sup>1</sup>H NMR (500 MHz, methanol-*d*<sub>4</sub>):  $\delta$  7.79 (d, *J* = 7.9 Hz, 1H), 7.70–7.63 (m, 2H), 7.58–7.48 (m, 2H), 7.45–7.35 (m, 2H), 4.02 (t, *J* = 6.5 Hz, 2H), 3.96 (s, 3H), 3.70–3.61 (m, 2H), 3.00 (t, *J* = 5.4 Hz, 2H), 2.79 (t, *J* = 5.3 Hz, 2H), 2.04–1.85 (m, 8H). <sup>13</sup>C NMR (126 MHz, methanol-*d*<sub>4</sub>):  $\delta$  158.74, 157.04, 151.00, 139.40, 134.19, 129.18, 126.29, 125.40, 124.43, 123.92, 121.71, 118.90, 115.20, 113.25, 104.61, 56.77, 47.78, 29.30, 28.99, 26.31, 26.02, 23.18, 21.79. HRMS: [M+H]<sup>+</sup> 433.2056 (calculated for [C<sub>25</sub>H<sub>29</sub>N<sub>4</sub>OS]<sup>+</sup>: 433.2017).

**N<sup>6</sup>-(1,3-Benzothiazol-2-yl)-N<sup>1</sup>-(7-methoxy-1,2,3,4-tetrahydroacridin-9-yl)hexane-1,6-diamine Hydrochloride (HK 1070).** Yield 27%; mp 151.7–152.6 °C; purity 99%. <sup>1</sup>H NMR (500 MHz, methanol-*d*<sub>4</sub>):  $\delta$  7.81 (d, *J* = 8.0 Hz, 1H), 7.73 (d, *J* = 9.3 Hz, 1H), 7.69 (d, *J* = 2.6 Hz, 1H), 7.58 (dd, *J* = 8.1, 1.1 Hz, 1H), 7.55–7.49 (m, 2H), 7.41–7.36 (m, 1H), 3.99–3.94 (m, 5H), 3.58 (t, *J* = 7.0 Hz, 2H), 3.04–2.99 (m, 2H), 2.77 (t, *J* = 5.8 Hz, 2H), 1.95 (p, *J* = 3.1 Hz, 4H), 1.92–1.85 (m, 2H), 1.85–1.78 (m, 2H), 1.61–1.50 (m, 4H). <sup>13</sup>C NMR (126 MHz, methanol-*d*<sub>4</sub>):  $\delta$  158.65, 157.20, 150.74, 139.48, 134.48, 129.23, 126.29, 125.40, 123.92, 121.75, 118.69, 115.15, 112.92, 105.02, 56.62, 48.52, 31.81, 29.25, 29.14, 27.42, 27.33, 25.66, 23.17, 21.86. HRMS: [M+H]<sup>+</sup> 461.2366 (calculated for [C<sub>27</sub>H<sub>33</sub>N<sub>4</sub>OS]<sup>+</sup>: 461.2330).

**N<sup>8</sup>-(1,3-Benzothiazol-2-yl)-N<sup>1</sup>-(7-methoxy-1,2,3,4-tetrahydroacridin-9-yl)octane-1,8-diamine Hydrochloride (HK 1072).** Yield 15%; mp 146.8–147.4 °C; purity 99%. <sup>1</sup>H NMR (500 MHz, methanol-*d*<sub>4</sub>):  $\delta$  7.78 (d, *J* = 7.8 Hz, 1H), 7.74 (d, *J* = 9.2 Hz, 1H), 7.65 (d, *J* = 2.5 Hz, 1H), 7.60–7.54 (m, 1H), 7.52–7.44 (m, 2H), 7.38–7.31 (m, 1H), 3.96 (s, 3H), 3.95–3.88 (m, 2H), 3.57 (t, *J* = 7.1 Hz, 2H), 3.06–2.98 (m, 2H), 2.79–2.70 (m, 2H), 1.99–1.90 (m, 4H), 1.88–1.74 (m, 4H), 1.55–1.36 (m, 8H). <sup>13</sup>C NMR (126 MHz, methanol-*d*<sub>4</sub>):  $\delta$  158.50, 157.04, 150.57, 139.82, 134.39, 129.05, 126.07, 125.33, 124.59, 123.81, 121.73, 118.54, 115.24, 112.76, 104.93, 56.65, 48.59, 31.95, 30.15, 30.07, 29.22, 27.66, 27.63, 25.62, 23.14, 21.84. HRMS: [M+H]<sup>+</sup> 489.2682 (calculated for [C<sub>29</sub>H<sub>37</sub>N<sub>4</sub>OS]<sup>+</sup>: 489.2683).

**In Vitro Lysozyme Amyloid Aggregation: ThT Fluorescence Assay.** HEWL was dissolved in 70 mM glycine buffer with an addition of 80 mM NaCl at pH 2.7 to a final concentration of 10  $\mu$ M. The HEWL solution was incubated at 65 °C for 2 h and stirred at 1200 rpm in thermomixer. After the incubation, the amyloid-specific dye ThT was added, and samples were incubated for another 60 min at 37 °C in dark. The formation of HEWL amyloid fibrils was confirmed by a significant increase in the ThT fluorescence. Measurements were performed in a 96-well plate using a Synergy MX (BioTek) spectrofluorimeter. The excitation wavelength was set at 440 nm and the emission recorded at 485 nm. The excitation and emission slits were adjusted to 9.0/9.0 nm, and the top probe vertical offset was 6 mm.

**Effect of Compounds on HEWL Amyloid Fibrillization: Determination of IC<sub>50</sub> Values.** Interference of BTZ, 7-MEOTA, and HK compounds with an amyloid aggregation of HEWL was studied using ThT fluorescence assay in the concentration range of 100 pM to 1 mM at the fixed 10  $\mu$ M protein concentration. All compounds were dissolved in DMSO. To clarify the possible binding competition between ThT and studied compounds, we performed an additional experiment described in detail in the SI (*Control experiment - clarification of the potential competitive binding among ThT and studied compounds, Figure S10*). The recorded ThT fluorescence intensities were normalized to the ThT fluorescence of lysozyme amyloid fibrils in the absence of studied compounds.

**Atomic Force Microscopy (AFM).** Samples for AFM were applied on freshly cleaved mica. After 5 min adsorption period the surface of mica was rinsed several times with ultrapure water and left to dry. AFM images were obtained using a scanning probe microscope

(Veeco di Innova) in a tapping mode using the NCHV cantilever with a specific resistance 0.01–0.025  $\Omega\text{-cm}^{-1}$ . All images are unfiltered.

**Attenuated Total Reflectance Fourier Transform Infrared (ATR-FTIR) Spectroscopy.** ATR-FTIR spectra were recorded using a Nicolet 8700 Fourier transform infrared spectrometer (Thermo Fisher Scientific) equipped with Smart OMNI-Sampler (diamond crystal). 5  $\mu$ L of themple (50  $\mu$ M HEWL, 500  $\mu$ M compound) was spread on the diamond surface. Each spectrum represents an average of 254 repetitions, recorded at the resolution of 2  $\text{cm}^{-1}$  in amide I region (1700–1600  $\text{cm}^{-1}$ ). Recorded spectra were smoothed using OMNIC 8 software (Thermo Fisher Scientific) to achieve the quality of spectra adequate for deconvolution. 11-point Savitzky–Golay filter (10.607  $\text{cm}^{-1}$ ) followed by 7-point Savitzky–Golay filter (6.750  $\text{cm}^{-1}$ ) was applied. Spectra were subsequently deconvoluted by peak analyzer in OriginPro 8 software (OriginLab Corp.). Baseline was subtracted, and the positions of peaks in amide I region were added manually in correlation with the raw data. To assign peak positions to the secondary structures, measurements were compared against the published literature.<sup>41</sup> Gaussian peak function was used to fit the data, and particular secondary structures content was obtained by Gaussian curves area integration.

**Statistical Analysis.** All experiments were performed at least in triplicate, and the presented data are expressed as the mean values with average deviation of *n* independent measurements (*n* ≥ 3). Specific *n* values are reported in the figure legends. IC<sub>50</sub> values (compound concentration with 50% inhibitory activity) were determined from curves obtained by fitting the average values with nonlinear least-squares method (Sigmoid, Parameter 3 in the SigmaPlot software (Systat Software Inc., USA)) using the equation  $y + a/(1 + \exp(+(\mathbf{x} - \mathbf{x}_0)/b))$ , where  $\mathbf{x}_0$  corresponds to the IC<sub>50</sub> value. The FTIR spectra of amide I region (1700–1600  $\text{cm}^{-1}$ ) represent an average of 254 repetitions. The content of the secondary structures was obtained by deconvolution of the spectra using peak analyzer in OriginPro 8 (OriginLab Corp.), namely the Gaussian peak function allowing determination of the particular secondary structure content (%) by Gaussian curves area integration. The precision of deconvolution fit is given by correlation coefficient adjusted R<sup>2</sup> in Table S1.

**Receptor and Ligands: In Silico Methods.** The structure of HEWL monomer was taken from Protein Data Bank with PDB ID 193L<sup>42</sup> at pH 4.3. Then, using PDB2PQR<sup>43</sup> server with Amber force field and PROPKA,<sup>44,45</sup> the pH calculation was performed to decrease the pH to 2.7, and the obtained structure is shown in Figure 10A. There are four disulfide bonds between residues C6–C127, C30–C115, C64–C80, and C76–C94 in this structure; therefore, four S–S bonds were added into the simulation to preserve these bonds.

Marvin Sketch 17.24 was used to get 3D structures of HK compounds at pH 2.7 (Figure 10B), at which IC<sub>50</sub> values have been experimentally determined. The structures of six compounds including 7-MEOTA, BTZ, HK 1066, HK 1068, HK 1070, and HK 1072 were optimized using Gaussian 09 software<sup>46</sup> at the B3LYP/6-31G(d) level of theory.

**Docking Method.** AutoDock Tools 1.5.4<sup>47</sup> was used to prepare the input for docking simulation with PDBQT format. Then, six compounds were docked to the receptor by using AutoDock Vina 1.2.<sup>48</sup> For global search, the exhaustiveness value was set to 800 to get reliable results. Ten modes of flexible ligand were generated, and the receptor dynamics was neglected. The lowest binding energy in the best docking mode was selected as the scoring function for the binding affinity.

**Molecular Dynamics (MD) Simulation.** The MD simulation was performed using GROMACS 2019.<sup>49,50</sup> The receptor–ligand structure obtained in the best docking mode was utilized as input for MD simulation with the AMBER99SB-ILN force field.<sup>51</sup> Parameters of ligand that characterize bond, angle, and dihedral, improper, and nonbonded interactions were computed using Antechamber<sup>52</sup> and Acrylpe<sup>53</sup> based on the General Amber Force Field (GAFF).<sup>54</sup> Atomic point charges were determined by AM1-BCC.<sup>55</sup>

The protein–ligand complexes were solvated in a cubic box by water molecules using the TIP3P model.<sup>56</sup> Then, counterions were

added to neutralize the system. After that, a concentration of 70 mM glycine and 80 mM NaCl was added to simulate the experimental conditions. The leapfrog algorithm<sup>57</sup> was used to integrate equations of motion with a time step of 2 fs. The LINCS algorithm was utilized to constrain bonds.<sup>58</sup> Systems were minimized using the steepest descent algorithm. Then, they were equilibrated in NVT for 500 ps and NPT for 5 ns ensembles at 298 K and 1 atm. The temperature and pressure were maintained by the v-rescale thermostat<sup>59</sup> and Parrinello–Rahman barostat.<sup>60</sup> A cutoff of 1.2 nm was used to estimate the van der Waals (vdW) force, while the long-range electrostatic interaction was calculated using the particle mesh Ewald (PME) method.<sup>61</sup> A 100 ns MD simulation was performed, and the snapshots were recorded every 10 ps at equilibrium.

**Molecular Mechanics Poisson–Bolzmann Surface Area (MM-PBSA) Method.** In the MM-PBSA method,<sup>62</sup> which was presented in more detail in previous studies,<sup>63–65</sup> the binding free energy of ligand to the receptor is given by the following equation,

$$\Delta G_{\text{bind}} = \Delta E_{\text{elec}} + \Delta E_{\text{vdw}} + \Delta G_{\text{SA}} + \Delta G_{\text{PB}} - T\Delta S \quad (1)$$

where  $\Delta E_{\text{elec}}$ ,  $\Delta E_{\text{vdw}}$ ,  $\Delta G_{\text{SA}}$ , and  $\Delta G_{\text{PB}}$  are the electrostatic, vdW, nonpolar, and polar solvation energies, respectively. The electrostatic and vdW interaction energies were calculated using the same parameters as the MD simulations. The nonpolar solvation energy was obtained by the formula  $\Delta G_{\text{SA}} = \gamma \text{SASA}$ , where SASA stands for solvate-accessible surface area ( $\text{\AA}^2$ ), calculated from the SASA tool in the GROMACS package and  $\gamma = 0.0072 \text{ kcal}\cdot\text{mol}^{-1}\text{\AA}^{-2}$ .<sup>66</sup> The polar solvation energy was calculated using the APBS package.<sup>67</sup> The entropy contribution,  $-T\Delta S$ , was obtained using the method proposed by Duan et al.<sup>68</sup>

**Tools and Measures Used for Data Analysis.** Root-mean-square deviation (RMSD) was calculated as the deviation of the C-alpha atoms of the receptor from the initial structure. A hydrogen bond (HB) was formed if the distance between donor D and acceptor A is  $<3.5 \text{ \AA}$ , the H–A distance is  $<2.7 \text{ \AA}$ , and the D–H–A angle is  $>135^\circ$ . A nonbonded contact (NBC) is a noncovalent bonded contact other than a HB. It is defined as the contact between the C or S atom of a ligand and any atom of a protein or water molecule when they are at a distance of  $2.9$ – $3.9 \text{ \AA}$ . The HBs and NBCs were analyzed using LigPlot++ version 1.44.<sup>69</sup>

**Nuclear Magnetic Resonance (NMR).** All NMR experiments were done at 25 °C either on a Bruker Avance III 500 MHz equipped with a 5 mm SMART probe or 700 MHz NMR spectrometer equipped with the RT probe. HEWL samples (500  $\mu\text{M}$ ) were prepared using 10 mM citrate–phosphate buffer with 100 mM NaCl (pH 2.8), and 10% D<sub>2</sub>O was added for locking purpose. DSS was used as an internal standard (0.00 ppm). HK 1066 and HK 1072 were first dissolved in DMSO-*d*<sub>6</sub> and then diluted into the same buffer for all the experiments. Two-dimensional (<sup>1</sup>H) total correlation spectroscopy (2D TOCSY) and nuclear Overhauser spectroscopy (2D NOESY) were recorded for HEWL in free and bound (1:1 HEWL and ligand) forms with a mixing time of 80 and 150 ms, respectively, and the spectral width was set to 15 ppm in both directions. One dimensional STD NMR was performed using 1 mM concentration of ligand molecules.

The chemical shifts of the HEWL from 2D 1H-1H TOCSY (mixing time 80 ms) and NOESY (mixing time 150 ms) experiments were assessed and compared with the reference chemical shift,<sup>70</sup> deposited in BMRB. The identity of the chemical shifts of the HEWL residues interacting with HK compounds obtained from MD simulation study has been also subsequently cross validated.

STD NMR spectra were acquired at a ligand/HEWL mixture ratio of 300:1. Selective irradiation of HEWL was achieved by a train of Gaussian-shaped pulses with a 1% truncation and each of 49 ms in duration and separated by a 1 ms delay. A total of 40 selected pulses were applied, leading to a total time of saturation of 2 s. The so-called on resonance for HEWL was fixed at 0.2 ppm, and off-resonance was at 40 ppm, where neither protein nor the ligand resonances were present. Subtraction of the two spectra (on-resonance–off-resonance) by phase cycling leads to the difference spectrum that contains signals arising from the saturation transfer. The reference spectrum was

recorded with 640 scans, while the difference spectrum was obtained with 1280 scans. Data processing was performed using TOPSPIN program suite for all the spectra, and peak assignment was done using the SPARKY software.

## ASSOCIATED CONTENT

### Supporting Information

The Supporting Information is available free of charge at <https://pubs.acs.org/doi/10.1021/acschemneuro.9b00419>.

FTIR peak analysis, deconvolution and secondary structure percentage distributions; list of residues forming nonbonded contacts with HK compounds; 3D images of docking poses and contact networks of studied compounds; correlations between docking binding energy, binding free energy (MM-PBSA), IC<sub>50</sub> values,  $\Delta G_{\text{exp}}$ , and time dependence of C $\alpha$  RMSD of lysozyme bound to studied molecules; and control experiment – clarification of the potential competitive binding among ThT and studied compounds, including Figures S1–S10 and Tables S1–S3 (PDF)

## AUTHOR INFORMATION

### Corresponding Authors

Mai Suan Li – Institute of Physics, Polish Academy of Sciences, 02-668 Warsaw, Poland;  [orcid.org/0000-0001-7021-7916](https://orcid.org/0000-0001-7021-7916); Phone: +(48 22) 843 70 01 (3326); Email: [masli@ifpan.edu.pl](mailto:masli@ifpan.edu.pl)

Zuzana Gazova – Department of Biophysics, Institute of Experimental Physics, Slovak Academy of Sciences, 040 01 Kosice, Slovakia;  [orcid.org/0000-0002-0670-3431](https://orcid.org/0000-0002-0670-3431); Phone: +421 (055) 720 (4135); Email: [gazova@saske.sk](mailto:gazova@saske.sk)

### Authors

Miroslav Gancar – Department of Biophysics, Institute of Experimental Physics, Slovak Academy of Sciences, 040 01 Kosice, Slovakia

Kiet Ho – Life Science Lab, Institute of Computational Science and Technology, Quang Trung Software City, Ho Chi Minh City 700000, Vietnam

Sk. Abdul Mohid – Department of Biophysics, Bose Institute, Centenary Campus, West Bengal 700054, Kolkata, India

Nguyen Quoc Thai – Dong Thap University, Cao Lanh City 700000, Dong Thap, Vietnam

Zuzana Bednarikova – Department of Biophysics, Institute of Experimental Physics, Slovak Academy of Sciences, 040 01 Kosice, Slovakia

H. Linh Nguyen – Life Science Lab, Institute of Computational Science and Technology, Quang Trung Software City, Ho Chi Minh City 700000, Vietnam

Anirban Bhunia – Department of Biophysics, Bose Institute, Centenary Campus, West Bengal 700054, Kolkata, India;  [orcid.org/0000-0002-8752-2842](https://orcid.org/0000-0002-8752-2842)

Eugenie Nepovimova – Department of Chemistry, Faculty of Science, University of Hradec Kralove, 500 03 Hradec Kralove, Czech Republic

Complete contact information is available at: <https://pubs.acs.org/doi/10.1021/acschemneuro.9b00419>

### Author Contributions

M.S.L. and Z.G. conceived the experiments. Z.G., Z.B., and M.G. designed *in vitro* experiments and analyzed results; M.G. and Z.B. performed *in vitro* experiments. M.S.L. designed *in silico* experiments; K.H., N.Q.T., and H.L.N. performed *in silico*

experiments. S.A.M. and A.B. designed and performed NMR experiments and analyzed the data. E.N. synthesized the HK compounds. Z.G. and M.G. wrote the paper; all authors reviewed the manuscript.

#### Author Contributions

<sup>†</sup>M.G. and K.H. contributed equally.

#### Notes

The authors declare no competing financial interest.

#### ACKNOWLEDGMENTS

This work was supported by research grant projects in the frame of VEGA 2/0145/17, MVTS COST 083/14 action BM1405, and APVV-18-0284, the project Excellence of the University of Hradec Kralove, Polish NCN grant 2015/19/B/ST4/02721, Poland, project B2019.SPD.03, and Department of Science and Technology, Ho Chi Minh City, Vietnam. This research was partially supported in by PLGrid Infrastructure, and the supercomputer center TASK in Gdansk, Poland, and partially supported by the Council of Scientific and Industrial Research (02(0292)/17/EMR-II), Govt. of India to Dr. Anirban Bhunia.

#### REFERENCES

- (1) Dobson, C. M. (2003) Protein Folding and Misfolding. *Nature* 426 (6968), 884–890.
- (2) Abbaskhani, Z. (2016) Effect of Metal Ions on Aggregation of Amyloid Beta Peptide. *Parkinsonism Relat. Disord.* 22, No. e191.
- (3) Khlistunova, I., Biernat, J., Wang, Y., Pickhardt, M., von Bergen, M., Gazova, Z., Mandelkow, E., and Mandelkow, E.-M. (2006) Inducible Expression of Tau Repeat Domain in Cell Models of Tauopathy. *J. Biol. Chem.* 281 (2), 1205–1214.
- (4) Sattianayagam, P. T., Gibbs, S. D. J., Rowczenio, D., Pinney, J. H., Wechalekar, A. D., Gilbertson, J. A., Hawkins, P. N., Lachmann, H. J., and Gillmore, J. D. (2012) Hereditary Lysozyme Amyloidosis - Phenotypic Heterogeneity and the Role of Solid Organ Transplantation. *J. Intern. Med.* 272 (1), 36–44.
- (5) Wang, S., Kestler, D., Coriu, D., Solomon, A., Murphy, C., Wooliver, C., and Weiss, D. (2007) Familial Amyloidosis Associated with a Novel Mutation (D68g) in the Lysozyme Gene, *XIIth International Symposium on Amyloidosis*, CRC Press, pp 208–210.
- (6) Mocanu, M.-M., Ganea, C., Siposova, K., Filippi, A., Demjen, E., Marek, J., Bednarikova, Z., Antosova, A., Baran, I., and Gazova, Z. (2014) Polymorphism of Hen Egg White Lysozyme Amyloid Fibrils Influences the Cytotoxicity in LLC-PK1 Epithelial Kidney Cells. *Int. J. Biol. Macromol.* 65, 176–187.
- (7) Ramazzotti, M., Melani, F., Marchi, L., Mulinacci, N., Gestri, S., Tiribilli, B., and Degl'Innocenti, D. (2016) Mechanisms for the Inhibition of Amyloid Aggregation by Small Ligands. *Biosci. Rep.* 36 (5), No. e00385.
- (8) Reinke, A. A., and Gestwicki, J. E. (2007) Structure?Activity Relationships of Amyloid Beta-Aggregation Inhibitors Based on Curcumin: Influence of Linker Length and Flexibility. *Chem. Biol. Drug Des.* 70 (3), 206–215.
- (9) Simone Tranches Dias, K., and Viegas, C. (2014) Multi-Target Directed Drugs: A Modern Approach for Design of New Drugs for the Treatment of Alzheimer's Disease. *Curr. Neuropharmacol.* 12 (3), 239–255.
- (10) de Freitas Silva, M., Dias, K. S. T., Gontijo, V. S., Ortiz, C. J. C., and Viegas, C. (2018) Multi-Target Directed Drugs as a Modern Approach for Drug Design Towards Alzheimer's Disease: An Update. *Curr. Med. Chem.* 25 (29), 3491–3525.
- (11) Ortega, G., Tavanti, F., Bednarikova, Z., Gazova, Z., Rigillo, G., Imbriano, C., Basile, V., Asti, M., Rigamonti, L., Saladini, M., et al. (2018) Curcumin Derivatives and A $\beta$ -Fibrillar Aggregates: An Interactions' Study for Diagnostic/Therapeutic Purposes in Neurodegenerative Diseases. *Bioorg. Med. Chem.* 26 (14), 4288–4300.
- (12) Doig, A. J., and Derreumaux, P. (2015) Inhibition of Protein Aggregation and Amyloid Formation by Small Molecules. *Curr. Opin. Struct. Biol.* 30, 50–56.
- (13) Shuaib, S., and Goyal, B. (2018) Scrutiny of the Mechanism of Small Molecule Inhibitor Preventing Conformational Transition of Amyloid- $\beta$  42 Monomer: Insights from Molecular Dynamics Simulations. *J. Biomol. Struct. Dyn.* 36 (3), 663–678.
- (14) Van Vuong, Q., Bednarikova, Z., Antosova, A., Huy, P. D. Q., Siposova, K., Tuan, N. A., Li, M. S., and Gazova, Z. (2015) Inhibition of Insulin Amyloid Fibrillation by Glyco-Acridines: An in Vitro and in Silico Study. *MedChemComm* 6 (5), 810–822.
- (15) Vuong, Q. V., Siposova, K., Nguyen, T. T., Antosova, A., Balogova, L., Drajna, L., Imrich, J., Li, M. S., and Gazova, Z. (2013) Binding of Glyco-Acridine Derivatives to Lysozyme Leads to Inhibition of Amyloid Fibrillization. *Biomacromolecules* 14 (4), 1035–1043.
- (16) Siddiqi, M. K., Alam, P., Chaturvedi, S. K., Khan, M. V., Nusrat, S., Malik, S., and Khan, R. H. (2018) Capreomycin Inhibits the Initiation of Amyloid Fibrillation and Suppresses Amyloid Induced Cell Toxicity. *Biochim. Biophys. Acta, Proteins Proteomics* 1866 (4), 549–557.
- (17) Gazova, Z., Siposova, K., Kurin, E., Mučaji, P., and Nagy, M. (2013) Amyloid Aggregation of Lysozyme: The Synergy Study of Red Wine Polyphenols. *Proteins: Struct., Funct., Genet.* 81 (6), 994–1004.
- (18) Summers, W. K. (2006) Tacrine, and Alzheimer's Treatments. *J. Alzheimer's Dis.* 9 (s3), 439–445.
- (19) Korabecny, J., Musilek, K., Holas, O., Binder, J., Zemek, F., Marek, J., Pohanka, M., Opletalova, V., Dohnal, V., and Kuca, K. (2010) Synthesis and in Vitro Evaluation of N-Alkyl-7-Methoxytacrine Hydrochlorides as Potential Cholinesterase Inhibitors in Alzheimer Disease. *Bioorg. Med. Chem. Lett.* 20 (20), 6093–6095.
- (20) Gazova, Z., Soukup, O., Sepsova, V., Siposova, K., Drtinova, L., Jost, P., Spilovska, K., Korabecny, J., Nepovimova, E., Fedunova, D., et al. (2017) Multi-Target-Directed Therapeutic Potential of 7-Methoxytacrine-Adamantylamine Heterodimers in the Alzheimer's Disease Treatment. *Biochim. Biophys. Acta, Mol. Basis Dis.* 1863 (2), 607–619.
- (21) Keri, R. S., Patil, M. R., Patil, S. A., and Budagumpi, S. (2015) A Comprehensive Review in Current Developments of Benzothiazole-Based Molecules in Medicinal Chemistry. *Eur. J. Med. Chem.* 89, 207–251.
- (22) Thai, N. Q., Bednarikova, Z., Gancar, M., Linh, H. Q., Hu, C.-K., Li, M. S., and Gazova, Z. (2018) Compound CID 9998128 Is a Potential Multitarget Drug for Alzheimer's Disease. *ACS Chem. Neurosci.* 9 (11), 2588–2598.
- (23) Kabsch, W., and Sander, C. (1983) Dictionary of Protein Secondary Structure: Pattern Recognition of Hydrogen-Bonded and Geometrical Features. *Biopolymers* 22 (12), 2577–2637.
- (24) Tu, L.-H., and Raleigh, D. P. (2013) Role of Aromatic Interactions in Amyloid Formation by Islet Amyloid Polypeptide. *Biochemistry* 52 (2), 333–342.
- (25) Mayer, M., and Meyer, B. (2001) Group Epitope Mapping by Saturation Transfer Difference NMR To Identify Segments of a Ligand in Direct Contact with a Protein Receptor. *J. Am. Chem. Soc.* 123 (25), 6108–6117.
- (26) Bhunia, A., Bhattacharjya, S., and Chatterjee, S. (2012) Applications of Saturation Transfer Difference NMR in Biological Systems. *Drug Discovery Today* 17 (9–10), 505–513.
- (27) Takai, E., Uda, K., Matsushita, S., Shikiya, Y., Yamada, Y., Shiraki, K., Zako, T., and Maeda, M. (2014) Cysteine Inhibits Amyloid Fibrillation of Lysozyme and Directs the Formation of Small Worm-like Aggregates through Non-Covalent Interactions. *Biotechnol. Prog.* 30 (2), 470–478.
- (28) Patel, P., Parmar, K., Patel, D., Kumar, S., Trivedi, M., and Das, M. (2018) Inhibition of Amyloid Fibril Formation of Lysozyme by Ascorbic Acid and a Probable Mechanism of Action. *Int. J. Biol. Macromol.* 114, 666–678.

- (29) Feng, S., Song, X.-H., and Zeng, C.-M. (2012) Inhibition of Amyloid Fibrillation of Lysozyme by Phenolic Compounds Involves Quinoprotein Formation. *FEBS Lett.* 586 (22), 3951–3955.
- (30) Lieu, V. H., Wu, J. W., Wang, S. S.-S., and Wu, C.-H. (2007) Inhibition of Amyloid Fibrillization of Hen Egg-White Lysozymes by Rifampicin and p-Benzoquinone. *Biotechnol. Prog.* 23 (3), 698–706.
- (31) Gazova, Z., Bellova, A., Daxnerova, Z., Imrich, J., Kristian, P., Tomascikova, J., Bagelova, J., Fedunova, D., and Antalik, M. (2008) Acridine Derivatives Inhibit Lysozyme Aggregation. *Eur. Biophys. J.* 37 (7), 1261–1270.
- (32) Re, F., Airolidi, C., Zona, C., Masserini, M., Ferla, B. La, Quattrochi, N., and Nicotra, F. (2010) Beta Amyloid Aggregation Inhibitors: Small Molecules as Candidate Drugs for Therapy of Alzheimers Disease. *Curr. Med. Chem.* 17 (27), 2990–3006.
- (33) Ulicna, K., Bednarikova, Z., Hsu, W.-T., Holztragerova, M., Wu, J. W., Hamulakova, S., Wang, S. S. S., and Gazova, Z. (2018) Lysozyme Amyloid Fibrillization in Presence of Tacrine/Acridone-Coumarin Heterodimers. *Colloids Surf., B* 166, 108–118.
- (34) Romero, A., Cacabelos, R., Oset-Gasque, M. J., Samadi, A., and Marco-Contelles, J. (2013) Novel Tacrine-Related Drugs as Potential Candidates for the Treatment of Alzheimer's Disease. *Bioorg. Med. Chem. Lett.* 23 (7), 1916–1922.
- (35) Nepovimova, E., Uliassi, E., Korabecny, J., Peña-Altamira, L. E., Samez, S., Pesaresi, A., Garcia, G. E., Bartolini, M., Andrisano, V., Bergamini, C., et al. (2014) Multitarget Drug Design Strategy: Quinone-Tacrine Hybrids Designed To Block Amyloid- $\beta$  Aggregation and To Exert Anticholinesterase and Antioxidant Effects. *J. Med. Chem.* 57 (20), 8576–8589.
- (36) Frare, E., Polverino de Laureto, P., Zurdo, J., Dobson, C. M., and Fontana, A. (2004) A Highly Amyloidogenic Region of Hen Lysozyme. *J. Mol. Biol.* 340 (5), 1153–1165.
- (37) Krebs, M. R. H., Wilkins, D. K., Chung, E. W., Pitkeathly, M. C., Chamberlain, A. K., Zurdo, J., Robinson, C. V., and Dobson, C. M. (2000) Formation and Seeding of Amyloid Fibrils from Wild-Type Hen Lysozyme and a Peptide Fragment from the  $\beta$ -Domain. *J. Mol. Biol.* 300 (3), 541–549.
- (38) Canet, D., Last, A. M., Tito, P., Sunde, M., Spencer, A., Archer, D. B., Redfield, C., Robinson, C. V., and Dobson, C. M. (2002) Local Cooperativity in the Unfolding of an Amyloidogenic Variant of Human Lysozyme. *Nat. Struct. Biol.* 9 (4), 308–315.
- (39) Korabecny, J., Dolezal, R., Cabelova, P., Horova, A., Hruba, E., Ricny, J., Sedlacek, L., Nepovimova, E., Spilovska, K., Andrs, M., et al. (2014) 7-MEOTA-Donepezil like Compounds as Cholinesterase Inhibitors: Synthesis, Pharmacological Evaluation, Molecular Modeling and QSAR Studies. *Eur. J. Med. Chem.* 82, 426–438.
- (40) Spilovska, K., Korabecny, J., Kral, J., Horova, A., Musilek, K., Soukup, O., Drtinova, L., Gazova, Z., Siposova, K., and Kuca, K. (2013) 7-Methoxytacrine-Adamantylamine Heterodimers as Cholinesterase Inhibitors in Alzheimer's Disease Treatment - Synthesis, Biological Evaluation and Molecular Modeling Studies. *Molecules* 18 (2), 2397–2418.
- (41) Yang, H., Yang, S., Kong, J., Dong, A., and Yu, S. (2015) Obtaining Information about Protein Secondary Structures in Aqueous Solution Using Fourier Transform IR Spectroscopy. *Nat. Protoc.* 10 (3), 382–396.
- (42) Vaney, M. C., Maignan, S., Riès-Kautt, M., and Ducruix, A. (1996) High-Resolution Structure (1.33 Å) of a HEW Lysozyme Tetragonal Crystal Grown in the APCF Apparatus. Data and Structural Comparison with a Crystal Grown under Microgravity from Space Hab-01 Mission. *Acta Crystallogr., Sect. D: Biol. Crystallogr.* 52 (3), S05–S17.
- (43) Dolinsky, T. J., Nielsen, J. E., McCammon, J. A., and Baker, N. A. (2004) PDB2PQR: An Automated Pipeline for the Setup of Poisson-Boltzmann Electrostatics Calculations. *Nucleic Acids Res.* 32 (1), W665–W667.
- (44) Søndergaard, C. R., Olsson, M. H. M., Rostkowski, M., and Jensen, J. H. (2011) Improved Treatment of Ligands and Coupling Effects in Empirical Calculation and Rationalization of pK<sub>a</sub> Values. *J. Chem. Theory Comput.* 7 (7), 2284–2295.
- (45) Olsson, M. H. M., Søndergaard, C. R., Rostkowski, M., and Jensen, J. H. (2011) PROPKA3: Consistent Treatment of Internal and Surface Residues in Empirical pK<sub>a</sub> Predictions. *J. Chem. Theory Comput.* 7 (2), 525–537.
- (46) Frisch, M. J., Trucks, G. W., Schlegel, H. B., Scuseria, G. E., Robb, M. A., Cheeseman, J. R., Scalmani, G., Barone, V., Mennucci, B., and Petersson, G. A., et al. (2009) Gaussian 09, Revision B.01, Gaussian, Inc., Wallingford, CT.
- (47) Sanner, M. F. (1999) Python: A Programming Language for Software Integration and Development. *J. Mol. Graph. Model.* 17 (1), 57–61.
- (48) Trott, O., and Olson, A. J. (2009) AutoDock Vina: Improving the Speed and Accuracy of Docking with a New Scoring Function, Efficient Optimization, and Multithreading. *J. Comput. Chem.* 31 (2), 455–461.
- (49) Abraham, M. J., Murtola, T., Schulz, R., Páll, S., Smith, J. C., Hess, B., and Lindahl, E. (2015) GROMACS: High Performance Molecular Simulations through Multi-Level Parallelism from Laptops to Supercomputers. *SoftwareX* 1–2, 19–25.
- (50) Berendsen, H. J. C., van der Spoel, D., and van Drunen, R. (1995) GROMACS: A Message-Passing Parallel Molecular Dynamics Implementation. *Comput. Phys. Commun.* 91 (1–3), 43–56.
- (51) Hornak, V., Abel, R., Okur, A., Strockbine, B., Roitberg, A., and Simmerling, C. (2006) Comparison of Multiple Amber Force Fields and Development of Improved Protein Backbone Parameters. *Proteins: Struct., Funct., Genet.* 65 (3), 712–725.
- (52) Wang, J., Wang, W., Kollman, P. A., and Case, D. A. (2006) Automatic Atom Type and Bond Type Perception in Molecular Mechanical Calculations. *J. Mol. Graphics Modell.* 25 (2), 247–260.
- (53) Sousa da Silva, A. W., and Vranken, W. F. (2012) ACPYPE - AnteChamber PYthon Parser InterfacE. *BMC Res. Notes* 5 (1), 367.
- (54) Wang, J., Wolf, R. M., Caldwell, J. W., Kollman, P. A., and Case, D. A. (2004) Development and Testing of a General Amber Force Field. *J. Comput. Chem.* 25 (9), 1157–1174.
- (55) Jakalian, A., Jack, D. B., and Bayly, C. I. (2002) Fast, Efficient Generation of High-Quality Atomic Charges. AM1-BCC Model: II. Parameterization and Validation. *J. Comput. Chem.* 23 (16), 1623–1641.
- (56) Jorgensen, W. L., Chandrasekhar, J., Madura, J. D., Impey, R. W., and Klein, M. L. (1983) Comparison of Simple Potential Functions for Simulating Liquid Water. *J. Chem. Phys.* 79 (2), 926–935.
- (57) Hockney, R., Goel, S., and Eastwood, J. (1974) Quiet High-Resolution Computer Models of a Plasma. *J. Comput. Phys.* 14 (2), 148–158.
- (58) Hess, B., Bekker, H., Berendsen, H. J. C., and Fraaije, J. G. E. M. (1997) LINCS: A Linear Constraint Solver for Molecular Simulations. *J. Comput. Chem.* 18 (12), 1463–1472.
- (59) Bussi, G., Donadio, D., and Parrinello, M. (2007) Canonical Sampling through Velocity Rescaling. *J. Chem. Phys.* 126 (1), 014101.
- (60) Parrinello, M., and Rahman, A. (1981) Polymorphic Transitions in Single Crystals: A New Molecular Dynamics Method. *J. Appl. Phys.* 52 (12), 7182–7190.
- (61) Darden, T., York, D., and Pedersen, L. (1993) Particle Mesh Ewald: An N · log(N) Method for Ewald Sums in Large Systems. *J. Chem. Phys.* 98 (12), 10089–10092.
- (62) Kollman, P. A., Massova, I., Reyes, C., Kuhn, B., Huo, S., Chong, L., Lee, M., Lee, T., Duan, Y., Wang, W., et al. (2000) Calculating Structures and Free Energies of Complex Molecules: Combining Molecular Mechanics and Continuum Models. *Acc. Chem. Res.* 33 (12), 889–897.
- (63) Nguyen, T. T., Mai, B. K., and Li, M. S. (2011) Study of Tamiflu Sensitivity to Variants of A/H5N1 Virus Using Different Force Fields. *J. Chem. Inf. Model.* 51 (9), 2266–2276.
- (64) Ngo, S. T., and Li, M. S. (2012) Curcumin Binds to A $\beta$  1–40 Peptides and Fibrils Stronger Than Ibuprofen and Naproxen. *J. Phys. Chem. B* 116 (34), 10165–10175.
- (65) Thai, N. Q., Tseng, N.-H., Vu, M. T., Nguyen, T. T., Linh, H. Q., Hu, C.-K., Chen, Y.-R., and Li, M. S. (2016) Discovery of DNA

Dyes Hoechst 34580 and 33342 as Good Candidates for Inhibiting Amyloid Beta Formation: In Silico and in Vitro Study. *J. Comput.-Aided Mol. Des.* 30 (8), 639–650.

(66) Still, W. C., Tempczyk, A., Hawley, R. C., and Hendrickson, T. (1990) Semianalytical Treatment of Solvation for Molecular Mechanics and Dynamics. *J. Am. Chem. Soc.* 112 (16), 6127–6129.

(67) Jurrus, E., Engel, D., Star, K., Monson, K., Brandi, J., Felberg, L. E., Brookes, D. H., Wilson, L., Chen, J., Liles, K., et al. (2018) Improvements to the APBS Biomolecular Solvation Software Suite. *Protein Sci.* 27 (1), 112–128.

(68) Duan, L., Liu, X., and Zhang, J. Z. H. (2016) Interaction Entropy: A New Paradigm for Highly Efficient and Reliable Computation of Protein-Ligand Binding Free Energy. *J. Am. Chem. Soc.* 138 (17), 5722–5728.

(69) Laskowski, R. A., and Swindells, M. B. (2011) LigPlot+: Multiple Ligand-Protein Interaction Diagrams for Drug Discovery. *J. Chem. Inf. Model.* 51 (10), 2778–2786.

(70) Redfield, C., and Dobson, C. M. (1988) Sequential Proton NMR Assignments and Secondary Structure of Hen Egg White Lysozyme in Solution. *Biochemistry* 27 (1), 122–136.